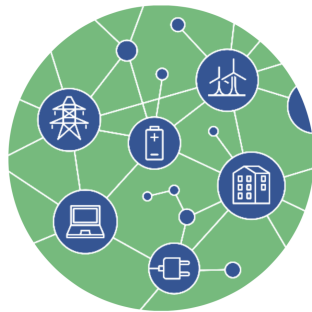




OPTIMAL SYSTEM-MIX OF FLEXIBILITY  
SOLUTIONS FOR EUROPEAN ELECTRICITY

# Overall Specifications of the Demonstrations

D3.2



**Contact: [www.osmose-h2020.eu](http://www.osmose-h2020.eu)**



The project has received funding from the European Union's Horizon 2020 research and innovation programme under grant agreement No 773406

## Document properties

### Project information

Programme	Optimal System-Mix Of Flexibility Solutions For European Electricity
Project Acronym	OSMOSE
Grant agreement	773406
Number of the Deliverable	D3.2
WP/Task related	3

### Document information

Document Name	<b>Overall Specifications of the Demonstrations</b>
Date of Delivery	June 28, 2019
Status and version	V1
Number of Pages	65

### Responsible

Responsible	Thibault Prevost (thibault.prevost@rte-france.com)
Authors	Thibault Prevost, Yannick Vernay, Carmen Cardozo, Guillaume Denis (RTE, La Défense, France), Yihui Zuo, Antonio Zecchino, Zhao Yuan, Rachid Cherkaoui, Mario Paolone (Distributed Electrical Systems Laboratory, EPFL, Lausanne, Switzerland), Markel Zubiaga Lazkano, Juan Jose Valera (Ingeteam R&D, Bilbao, Spain)
Reviewers	Unai Burdalo (REE, Spain), Lucas Orrù (Terna, Italy)
Approver	Nathalie Grisey (RTE, France)

### Dissemination level

Type (distribution level)	<b>PU Public</b>
	<del>CO — full consortium, Confidential, only for members of the consortium (including the Commission Services)</del>
	<del>CO — some partners, Confidential, only for some partners (list of partners to be defined)</del>

### Review history

Version	Date	Reviewer	Comment
V1	June 28, 2019		

## Table of content

<b>List of Acronyms</b>	<b>9</b>
<b>1 Introduction</b>	<b>10</b>
1.1 Motivations and scope . . . . .	10
1.2 Recall of WP3 objectives and schedule . . . . .	11
1.3 Outline of the deliverable . . . . .	12
1.4 Research questions and innovations . . . . .	13
<b>2 EPFL Demonstrations</b>	<b>14</b>
2.1 Technical description of the utility-scale BESS demonstrator . . . . .	14
2.1.1 EPFL MV grid description . . . . .	15
2.1.2 Communication protocols . . . . .	17
2.2 Technical description of the small-scale BESS demonstrator . . . . .	18
2.2.1 EPFL LV grid description . . . . .	18
2.2.2 Communication protocols . . . . .	19
2.3 Common data logging infrastructure . . . . .	21
2.4 Services, tests and performance metrics . . . . .	23
2.5 39-bus power system model for real time simulation . . . . .	24
2.5.1 Main component models . . . . .	24
2.5.2 BESS-VSC model . . . . .	28
2.5.3 Data logging infrastructure . . . . .	35
2.5.4 Test events and performance metrics for the real-time simulation . . . . .	35
<b>3 RingoLab Demo (RTE/Ingeteam)</b>	<b>36</b>
3.1 Presentation of Ringolab Overall specification . . . . .	36
3.1.1 Size and layout of the Ringolab Hardware platforms . . . . .	36
3.1.2 Location and RTE grid description . . . . .	37
3.1.3 Measures and data logging to support testing opportunities for Ringolab . . . . .	40
3.2 Implementing grid forming control in Ingeteam inverter . . . . .	42
3.2.1 Required control algorithm updates . . . . .	42
3.2.2 Performance validation through simulation of MIGRATE test-cases . . . . .	44
3.2.3 Discussion on MIGRATE control limits for RingoLab application . . . . .	48
3.3 DC side converter control developments . . . . .	49
3.3.1 Power sharing controls strategies for DC/DC converters . . . . .	50
3.3.2 Energy management controls for the HESS . . . . .	54
3.3.3 Service arbitrage for inverter capacity . . . . .	57
3.4 Additional grid-fault requirements . . . . .	58
3.4.1 Unbalance FRT requirements for grid-forming inverter . . . . .	58
3.4.2 Anti-islanding . . . . .	58
3.5 Test protocols . . . . .	59
3.5.1 Factory acceptance test . . . . .	59
3.5.2 On field test protocol . . . . .	60
3.6 Key performance indicators . . . . .	61
<b>4 Conclusion</b>	<b>62</b>

## List of Figures

1.1	Schedule of the demonstrations in Osmose WP3 . . . . .	12
2.1	The 720kVA/500 kWh grid-connected BESS installed at the EPFL campus . . . . .	14
2.2	Schematic representation of the connection of the utility-scale BESS to the EPFL grid . . . . .	15
2.3	Topology of the EPFL MV grid under study . . . . .	15
2.4	Master Controller of the large-scale BESS . . . . .	17
2.5	Slave Controller of the large-scale BESS . . . . .	17
2.6	Communication with the the BESS and converter . . . . .	18
2.7	The main circuit of the small-scale BESS . . . . .	18
2.8	Topology of the EPFL experimental LV microgrid . . . . .	20
2.9	Hardware setup of the small-scale BESS control . . . . .	20
2.10	The finite state machine diagram of small BESS converter control . . . . .	21
2.11	The adopted DESL-EPFL PMU . . . . .	22
2.12	Screenshot of the outlook of the <i>Grafana</i> monitoring interface employed for frequency regulation services via the utility-scale BESS at EPFL . . . . .	22
2.13	Diagrams of IEEE 39-bus dynamic power systems . . . . .	24
2.14	Diagram of the speed-governing system of the steam turbines. . . . .	25
2.15	Model of the speed governor of hydro turbine. . . . .	25
2.16	The IEEE DC1A excitation system. . . . .	26
2.17	Diagram of the EPRI LOADSYN dynamic load model. . . . .	27
2.18	Diagram of the wind plant's model . . . . .	27
2.19	Diagrams of back-to-back converter controllers used in the type-3 wind turbine model . . . . .	28
2.20	A BESS integrated into power system Config. II . . . . .	29
2.21	Diagram of BESS-VSC . . . . .	29
2.22	Diagram of grid-forming control . . . . .	30
2.23	Diagram of VSC control from MIGRATE . . . . .	30
2.24	Diagram of grid-feeding control . . . . .	31
2.25	Diagram of the adopted grid-feeding control embedding outer loop control for frequency control . . . . .	31
2.26	Three Time Constant Equivalent Circuit of the BESS . . . . .	31
2.27	Configuration of $SSM_{rts}$ . . . . .	32
2.28	IGBT-based three-level NPC converter . . . . .	34
2.29	IGBT-based three-level NPC converter model in RT simulation . . . . .	34
3.1	HESS layout . . . . .	36
3.2	Single line diagram of the Ingeteam demo . . . . .	37
3.3	Location of Le Castelet on a map . . . . .	37
3.4	Destination substation - Single Line Diagram . . . . .	38
3.5	Example of voltage and current measurement when switching on load . . . . .	39
3.6	Example of voltage harmonics measurement for a week . . . . .	39
3.7	Single phase fault (20 kV, 24/04/2019). Up: Line-to-neutral voltages, Low: Line currents . . . . .	40
3.8	Telecommunication infrastructure . . . . .	41
3.9	Model adaptation flow chart . . . . .	43
3.10	State machine implemented in Matlab-Simulink . . . . .	43
3.11	Synchronization process results obtained in Matlab-Simulink . . . . .	45
3.12	Single bus case study used to check the ability of the converter to operate in islanded mode (disconnected from the grid, Brk 2 =0). . . . .	45

3.13 Simulation results for case 1-A-1, converter and grid voltage. Results of the average MIGRATE model (thin curve) superimposed with the results of the new model (thick curve). . . . .	46
3.14 Simulation results for case 1-A-1, converter RST currents. Results of the average MIGRATE model (thin curve) superimposed with the results of the new model (thick curve). . . . .	46
3.15 Single bus case study used to check the ability to track references for the active power injection and the terminal voltage. . . . .	46
3.16 Simulation results for case 1-B-2, converter and grid voltage. Results of the average MIGRATE model (thin curve) superimposed with the results of the new model (thick curve). . . . .	47
3.17 Simulation results for case 1-B-2, grid current module. Results of the average MIGRATE model (thin curve) superimposed with the results of the new model (thick curve). . . . .	47
3.18 Single bus case study used to check the stability and the ability to withstand large transients after a short circuit fault. . . . .	47
3.19 Simulation results for case 2-A-1, converter and grid voltage. Results of the average MIGRATE model (thin curve) superimposed with the results of the new model (thick curve). . . . .	48
3.20 Simulation results for case 2-A-1, converter and grid current modules. Results of the average MIGRATE model (thin curve) superimposed with the results of the new model (thick curve). . . . .	48
3.21 Current module at severe voltage unbalances . . . . .	49
3.22 Converter output current while virtual resistor is operating as a non-sinusoidal load. . . . .	49
3.23 Bloc diagram of Fixed battery + Supercapacitor regulating voltage . . . . .	50
3.24 Virtual RC scheme for transient sharing of the DC power . . . . .	51
3.25 DC/DC converters response for an active power step same values for both DC/DC (arbitrary choice) . . . . .	52
3.26 DC/DC converters response for an active power step $Cv1=Cv2$ and $Kd1=Kd2/2$ . . . . .	52
3.27 DC/DC converters response for an active power step $Cv1=Cv2/2$ and $Kd1=Kd2$ . . . . .	52
3.28 response of the scheme to active power step . . . . .	53
3.29 Bloc diagram of the PIP controller . . . . .	53
3.30 Active power of AC/DC converter, supercapacitor and Battery following: a angle step change of 0.1 rad (left), frequency step change of 0.01 p.u (right) . . . . .	54
3.31 Angle step change with (solid line) and w/o (dotted line) Energy control . . . . .	55
3.32 On a typical day for frequency . . . . .	56
3.33 Power output of an inverter providing different services. . . . .	57
3.34 Main scheme of the simulation and test process . . . . .	59
3.35 Grid emulator hardware and main characteristics . . . . .	60

## List of Tables

1.1	List of grid services that should be possible with the HESS . . . . .	11
2.1	Large-scale BESSs . . . . .	16
2.2	Small-scale BESSs . . . . .	19
2.3	List of Generation Units . . . . .	25
2.4	Parameters of 560 kWh Lithium Titanate Oxide BESS available at the EPFL-DESL . .	32
2.5	Parameters of one battery pack of the $BESS_{rts}$ . . . . .	33
2.6	Parameters for VSC . . . . .	33
3.1	Main characteristics . . . . .	36
3.2	Short-circuit currents simulated at the point of common coupling of the HESS . . . . .	38
3.3	Harmonic requirements on transmission grid by RTE . . . . .	40
3.4	Anti-islanding protection for distributed generation (H4 norm, french grid-code [1]) . .	59

## Executive Summary

Task 3.2 deals with the technical specifications of the 3 demonstrators foreseen in OSMOSE WP3:

1. an utility-scale battery energy storage system (BESS) at EPFL (Lausanne, Switzerland),
2. a small scale BESS also located at EPFL campus,
3. an hybrid energy storage system (HESS) connected to the RTE grid (RingoLab in France).

One of the main goals of these demonstrators is to assess the required conditions to implement the grid forming controls proposed in MIGRATE project considering different infrastructures and operational environments. For this purposes, the two demonstrators considered at EPFL are based on existing facilities, while RingoLab will be specifically built for the project using off-the-shelf equipment. In the former cases, first investigations were focus on the possibility of upgrading an existing control. In the latter case, efforts were devoted to the definition of the HESS technical specifications and to the development of its control in close collaboration between RTE and Ingeteam.

This report first presents the technical description of the EPFL demos and secondly the final specification of RingoLab. In both cases, the characteristics of the connection grids are included:

1. The utility-scale BESS consists in a 720 kVA/560 kWh Lithium-Titanate (LTO), equipped with a 720 kVA 4-quadrant converter, and connected to a 20 kV radial feeder of the EPFL campus medium voltage (MV) grid via a 630 kVA 3-phase transformer. This grid has an aggregated peak power consumption of about 300 kW and is equipped with 95 kWp of PV rooftop installations which make it a suitable test bed prone to highly variable voltage and current profiles.
2. The small scale BESS is a LTO battery with 25 kWh capacity, equivalent to one string of the utility-scale BESS, connected to a low voltage (400V) experimental microgrid through a 25 kVA 4-quadrant converter.
3. For RingoLab, we have specified a 1 MVA fully containerized solution based on a six lithium-ion battery racks (for 0.5 MW - 60min in total), six supercapacitors racks (1MW-10s), a 1 MVA low voltage inverter and a 0.6/20 kV transformer. It will be installed in the south of France and connected to the secondary of a 20 MVA 63/20 kV transformer serving an industrial load.

The choice of the selected substation (Castelet) was mainly driven by the availability of a 20kV connection point, which is not common in RTE network, while low short circuit ratio and load variability were desirable features. A transient fault recorder was installed at the 20 kV bus bar in February 2019. The analysis of a first measurement campaign let us think that the grid forming robustness will be challenged in operation as significant load changes and single-phase short circuits were recorded.

Regarding the modifications to the control of EPFL existing facilities, low level control layers were found to be closed in the utility-scale converter which prevent us from implementing the grid forming control as proposed in MIGRATE. To tackle this shortcoming, a solution to achieve grid-forming performances in this demonstrator through an outer loop is under investigation. The small-scale BESS offers full access to the converter control, so MIGRATE grid forming control can be implemented.

For RingoLab, Ingeteam has plugged the MIGRATE grid forming control to an electromagnetic model of the demonstrator specifically developed for the project. System performances were validated on MIGRATE test cases. However, some challenges remain regarding the behaviour of the grid forming algorithm and the current limitation strategy under unbalanced conditions such as asymmetrical faults. Possible solutions are under study. This report details control updates required for industrial implementation purposes and simulation results. In particular, detailed hardware limitations were implemented in the model at early stage of control design to accurately represent transient behaviour. Finally, different DC control strategies for power and energy sharing between the different DC components were described and simulated. The final choice will be made later on in the project.

This report also addresses some challenges related to the characterization of the robustness and effectiveness of the grid forming function. Indeed, grid forming was defined in MIGRATE to provide smoothing services to the frequency and the voltage amplitude. Specific DC controls will have the same effect on the battery output in a HESS setting. Here, we specify measurable key performance indicators taking into account the specific settings of each demonstrators.

These metrics include the well known RoCoF (Rate of Change of the Frequency) and the frequency nadir, but also the derivative of the active power and voltage, as well as the ratio between the battery and supercapacitor output variations. Therefore, details about the monitoring infrastructure and communication protocols are also provided at this stage of the project. Both EPFL grids are highly instrumented with PMUs. The data is collected in a dedicated server and Graphana open source tool will be used for analysis. RingoLab must be integrated to the RTE industrial telecommunication infrastructure, whose underlying constraints are taken into account while ensuring required monitoring and control capabilities of the demonstrator.

Finally, although multiservice control algorithms were discussed in the scope of Task 3.1, an insight on the compatibility of grid forming smoothing services with more classical ones, such as primary frequency control (PFC), is provided within the framework of the DC side energy management strategies. For instance, traditional PFC using storage systems may be challenging to achieve in practice as their state of charge may drift with the average system frequency. Mitigation measures must be put into place. For this purpose, a modified version of the IEEE 39 bus system has been modelled by EPFL in a real time simulation platform in order provide a reliable benchmark with long term testing capabilities. In addition, it will offer the possibility to compare grid forming solution with their grid following counterparts, for different scenarios (topology, renewable penetration, outage, etc.) and multiservices settings.

In conclusion, at the current stage of the project the objective are reached. Portability of the MIGRATE grid forming solution to the existing EPFL demonstrator and Ingeteam off-the-shelf equipment has been, to a sufficient extend, confirmed. RingoLab control, based on MIGRATE solution, is under development in collaboration between RTE and Ingeteam. Associated services and metrics to assess performances have been agreed and the required monitoring infrastructure is now deployed.

## List of Acronyms

<b>AS</b>	Ancillary Service
<b>AVR</b>	Automatic Voltage Regulator
<b>BESS</b>	Battery Energy Storage System
<b>DFIG</b>	Double Feed Induction Generator
<b>EMTP</b>	Electromagnetic Transients Program
<b>FAT</b>	Factory Acceptance Test
<b>FSM</b>	Finite State Machine
<b>HESS</b>	Hybrid Energy Storage System
<b>IGBT</b>	Isolated-Gate Bipolar Transistor
<b>KPI</b>	Key Performance Indicator
<b>LV</b>	Low Voltage
<b>MV</b>	Medium Voltage
<b>NPC</b>	Neutral-Point Clamped
<b>PFC</b>	Primary Frequency Control
<b>PLL</b>	Phase Locked Loop
<b>PMU</b>	Phasor Measurement Unit
<b>PCC</b>	Point Of Common Coupling
<b>PV</b>	Photovoltaics
<b>RingoLab</b>	Name of the RTE/Ingeteam demonstrator
<b>RMS</b>	Root Mean Square
<b>RoCoF</b>	Rate of Change of Frequency
<b>SC</b>	SuperCapacitor
<b>SCP</b>	Short Circuit Power
<b>SFC</b>	Secondary Frequency Control
<b>SOC</b>	State of Charge
<b>SRB</b>	Storage Rack Battery
<b>SRC</b>	Storage Rack Controller
<b>SRS</b>	Storage Rack System
<b>SSM</b>	State Space Model
<b>TFR</b>	Transient Fault Recorder
<b>TTC</b>	Three-time Constant
<b>VSC</b>	Voltage Source Converter

## 1 Introduction

The OSMOSE WP3 aims to test grid forming controls providing a synchronization service on medium size inverters and to validate its compatibility with other services in a real environment with a limited storage capacity.

It is recalled that a grid forming inverter is characterized by the following specific properties [2, 3]:

- behaves as a voltage source with limited frequency dynamics,
- synchronizes with other voltage source (if any),
- behaves properly in islanded mode (do not rely on direct frequency measurement),
- takes care of overcurrent limitation (being a voltage source as much as possible).

Therefore, grid forming inverters are expected to provide extra fast voltage control and frequency smoothing capabilities to the grid. These features entail new challenges with respect to traditionally used grid feeding controls as while behaving as a voltage source the inverter inherently exhibits high sensitivity to any change in grid impedance (load or topology). Hence, high level of robustness is needed to maintain the control in operation in various grid condition. The controls to be used in OSMOSE WP3 will comply with this requirement, bringing them to a next step of readiness and pushing the grid forming controls closer to a large scale implementation at the transmission level.

### 1.1 Motivations and scope

In the MIGRATE WP3 different grid forming algorithms have been developed, together with specific current limitation schemes. These controls have been tested in simulation and in laboratory environment with reduced scale hardware [2, 3]. The limitation of the lab tests are:

- ad hoc hardware design,
- the DC bus is a very stiff DC voltage source,
- the AC voltages are perfectly balanced,
- there is no harmonic distortion,
- deterministic disturbances are applied.

The demonstrators proposed in the OSMOSE WP3 will overcome these limitations.

On the one hand, different solutions will be considered in various settings: while RTE demonstrator will be built for this project based on off-the-shelf equipment, EPFL will upgrade existing devices in order to include the grid forming functionality. Moreover, the DC side will consist of whether a battery or an hybrid energy storage system (BESS - HESS) with a limited amount of energy.

On the other hand, by being connected to the existing distribution/transmission grids, the demonstrators will be subjected to a limited but non zero unbalance voltages, harmonic distortion, as well as grid disturbance. Therefore, in this project we will be able to assess the performances of at least the following features aside grid-forming:

- operation in real environment (sensitivity to harmonics/ unbalance) ,
- frequency smoothing,
- voltage amplitude smoothing,
- battery output smoothing using supercapacitors (in HESS),
- power and energy management in HESS in operation,
- effectiveness current limitation during transients,
- optimal use of the AC/DC inverter capacity with different DC device.

Moreover, the compatibility of this function with other services like primary and secondary frequency control, virtual line control or peak shaving control will be assessed. Though no universal definitions of those AC services exist, Table 1.1 shows a time scale distinction.

**Table 1.1:** List of grid services that should be possible with the HESS

Service Name	Service description	Response <sup>1</sup>	Maintain <sup>2</sup>
Frequency smoothing	Ensure that the local frequency signal has limited dynamics / limited RoCoF/ Avoid frequency discontinuities (phase jumps)	0-250ms	-
Fast frequency control	Adjust active power setpoint to fast frequency variation	250ms-2s	500ms-30s
Primary frequency control	Classical Frequency Containment Reserve	500ms-30s	15 min
V,f Control	Define the first voltage waves, allow islanding and autonomous operation	0-20 ms	-
Primary voltage control	Maintain the RMS voltage within specified limits around the setpoint	200ms-10 s	-
Secondary voltage control	Follow a voltage or reactive power setpoint	5-10 min	-
Secondary frequency control Energy, Reserve management	Adjust active power setpoint to external signal to bring frequency back to 50Hz	15 min	30 min - -
Virtual line / Congestion management	Charge / Discharge a couple of ESS, to emulate virtual flow between 2 nodes	1-10 s	30 min - a few hours
Peak shaving/ Load shifting/ Energy Arbitrage	Displace load demand within a day	1-10 s	30 min- a few hours

The multi-service approach will be explored in 2 frameworks: considering one unique storage device for all services (BESS demonstrators at EPFL site), and discriminating between dedicated facilities that provide specific services (HESS demonstrators at RTE grid). The latter will also provide an insight on the potential interest of having different DC players, owning different storage capabilities, jointly connected to the AC grid through a mutual inverter, in order to optimize its use.

## 1.2 Recall of WP3 objectives and schedule

- *O3a Enlarge the control strategy from MIGRATE to multi-service control algorithms implementable on storage installation, including the synchronization service and other more classical services such as primary frequency response and congestion management.*
- *O3b Test the robustness of the synchronization service to disturbances in current and voltage (large disturbances should induce smoothly saturated response, without disconnection).*
- *O3c Test the effectiveness of the synchronisation service in terms of reduction of local frequency deviation.*
- *O3d Demonstrate the portability of the control strategies over different hardware platforms: fast battery storage versus hybrid storage composed of supercapacitors and standard battery, as well as different converter products.*
- *O3e Quantify synergies to be expected from multi-service, in terms of sizing of installations.*
- *O3f Identify the highest level of inverter control where the synchronisation control algorithm can be implemented, which is important for portability.*

<sup>1</sup>Time to deployment of at least 90% - 95% of the required power, depending on the service and system.

<sup>2</sup>Time to keep requested power. It will depend on the scheduling time of the service and system.

To fulfill these objectives, task 3.2 considers the set up of different physical demonstrators at EPFL site and on RTE's grid. The storage system functions to be tested will largely depend on the demo location and surrounding grid, on the hardware composition of the demonstrator, and on metering and data infrastructure available. The overall schedule of the project is summarized in Fig. 1.1.

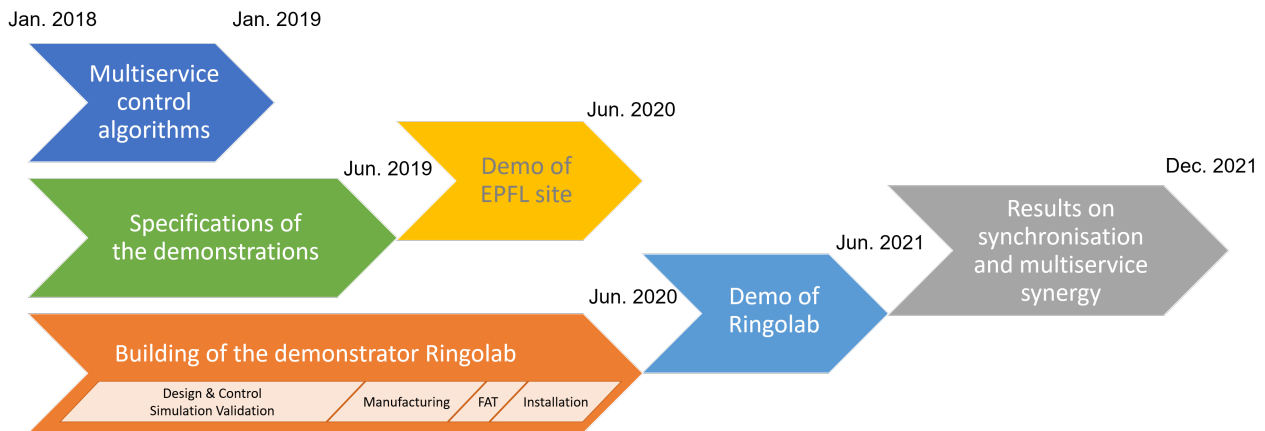


**Figure 1.1:** Schedule of the demonstrations in Osmose WP3

### 1.3 Outline of the deliverable

This deliverable presents the progress of the OSMOSE WP3, and more specifically Task 3.2. At current stage of the project a lot of effort has been put into modeling and on the technical specification of the demonstrators. Therefore, this deliverable presents details on a modified version of the IEEE 39 bus system set up by EPFL for real time simulation, as well as the Ingeteam implementation of the MIGRATE grid forming control and its current limitation strategy on their internal EMT inverter model. Preliminary results are supported by simulations.

Regarding demonstrators, this report includes:

- Overall technical description of the design and the connection grid, as well as the required metering and data infrastructures to support the experimentation.
- Required developments on communication protocols and control strategies.
- Desired functions and services to be implemented in the demonstrators.
- Test protocols and performance metrics for each functions and services to be tested.

Concretely, the document is organized as follows:

- Section 2 describes the two physical installations and the real time simulation model (IEEE 39 bus) set up at EPFL. One is a 720kVA lithium titanate BESS connected to the distribution grid of the university. The second demonstrators at EPFL is a reduced size BESS (25kW) on a separated microgrid. In both facilities, the performance of the grid-forming function will be assessed through a network of accurate PMUs.
- Section 3 details the hybrid storage system (HESS) to be built by Ingeteam in a RTE's substation. Preliminary simulation results show that the proposed solution exhibits robustness against grid disturbance. Main control design challenges are discussed. Key performance indicators (KPI) to assess the grid-forming effectiveness to smooth locally the frequency, and its ability to provide multi-services with deterministic allocation of each service to a dedicated storage unit are proposed.

---

## 1.4 Research questions and innovations

Since grid-connected grid-forming inverters are beyond the state-of-the-art, some developments have been required to remove the technical barriers and thus have brought significant scientific contributions. Main research questions addressed at the current stage of the project are listed below:

1. **Portability of MIGRATE grid forming to EPFL existing demonstrators.** MIGRATE grid forming control will be implemented in the small-scale BESS provided that the inner control loop of the converter can be coded. However, the inverter associated to the existing large scale BESS was originally designed for grid-feeding function and cannot be upgraded to include grid forming functionality as proposed in MIGRATE. The possibility of plugging an outer loop to achieve similar performances is under investigation.
2. **Portability of MIGRATE grid forming to Ingeteam commercial solution.** Off-line simulation showed satisfactory performances, but a more detailed model was needed to accurately predict the behaviour of the system during the first current peaks. Tackling this issue requires further investigation of the optimal setting of the hard blocking protection. In additions, challenges related to current limitation under unbalanced faults and grid-forming performance under harmonic disturbance need to be overcome in the following stage of the project.
3. **DC side energy management.** In RTE HESS a choice needs to be made on the most suitable strategy to manage the DC side and arbitrage between batteries and supercapacitors, as well as, keeping them charged for future needs. Different control strategies have been conceptually explored at this stage. More comprehensive simulations will be carried out afterwards.
4. **Multi-service approach, KPI, test protocols and data metering.** Several KPI have been defined to validate the performance of the services that the system will provide, these KPI have been developed taking into account the specific nature of each demonstration, available actuators and measurements.

These questions have been, at least partially, answered by the novel technical developments conducted at the time being and presented in this report to adapt grid-forming controls to the off-the-shell hardware, grid conditions and energy management strategies. Main results are listed below:

- Low-level **implementation of grid forming control algorithm on a commercial hardware** with open access to the code will offer the possibility of fair comparison between grid-feeding and grid-forming functions.
- For this purpose, **hardware limitations were taken into account at an early stage of control design** in order to limit the risk associated to the implementation of grid-forming function on off-the-shelf devices.
- Definition of the **transient grid forming control**. As aforementioned, in MIGRATE the DC side was considered as an ideal source. Here, the control algorithm has been updated to deal with the fact that the energy available in the storage is finite. The solution consists in making the inverter behave as a grid forming unit only for a short period after event occurs.
- Use of **distinguished DC physical storage system to perform different AC services**. Grid forming algorithms might require high power but limited energy to face fast network transients. On the contrary, the power assigned to provide frequency regulation services must be deployed for specific periods of time which may entail larger energy requirements. Different control strategies implementing this principle have been proposed.
- Open source development of **real time benchmark base on the IEEE 39-bus system** including an accurate BESS representation. This model will allow to scale up the OSMOSE WP3 findings and assessment of grid forming impact on the frequency of large power systems considering various grid configurations and wide range of uncertainties.

## 2 EPFL Demonstrations

Experimental demonstration activities at EPFL will allow the validation of the grid-forming controller and other grid services on real industry-grade hardware connected to realistic power distribution grids. For this purposes, two different testbeds available at EPFL are considered: a utility-scale battery energy storage system (BESS) and a smaller-scale one.

However, investigations on the inner controller of the converter associated to the larger BESS concluded that it does not allow to customize the VSC operation. Therefore, the experimental validation of the grid forming controller would be possibly carried-out only on the small-scale BESS. Then, synchronized PMUs will be used to assess the effectiveness of the implemented grid-forming controller.

In addition, real-time simulations will be performed on a modified version of IEEE 39-bus dynamic model in order to assess the performance of grid-forming BESSs and its impact on multi-services on larger grids considering different scenarios.

### 2.1 Technical description of the utility-scale BESS demonstrator

The utility-scale BESS installed at the EPFL campus consists in a 720 kVA/560 kWh Lithium-Titanate (LTO) battery technology, exhaustively utilized for a number of power grid support experimental activities [4]. This specific type of Lithium electrochemistry cells is among the most suitable for stationary grid application purposes, as it can perform up to 20,000 complete charge-discharge cycles at their maximum C-rate of 4C, being this index a representation of the amount of power flowing into/out from the battery over its nominal capacity. The BESS is equipped with a 720 kVA 4-quadrant converter which can operate in current source control mode (CSC, or grid-feeding) or in voltage source control mode (VSC, or manufacturer grid-forming with setpoints that can be changed via communication protocol 2.1.2). A view of the experimental BESS is shown in Fig. 2.1.



**Figure 2.1:** The 720kVA/500 kWh grid-connected BESS installed at the EPFL campus

### 2.1.1 EPFL MV grid description

The utility-scale BESS is connected to the EPFL campus medium voltage (MV) grid via a 630 kVA 3-phase MV/LV transformer, which raises the phase-to-phase voltage from 0.3 kV to 20 kV (see Fig. 2.2). This network is a particularly challenging distribution network where all the peculiarities of modern active distribution networks are stressed. The lines are short (most of them below 100 m), and the load demand is largely variable in function of the hour of the day and the weather conditions.

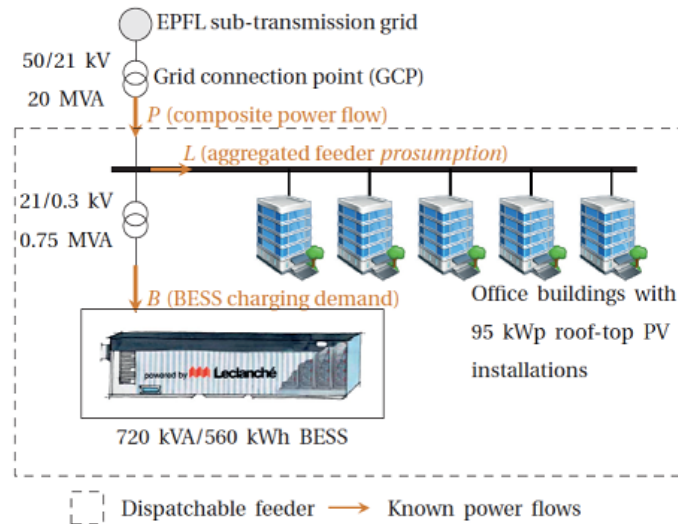


**Figure 2.2:** Schematic representation of the connection of the utility-scale BESS to the EPFL grid

Moreover, local power generation is present by means of 2 MW from photovoltaic (PV) technologies and 6 MW from combined heat and power generation units. More specifically, five office buildings of the EPFL campus are connected to the radial 20 kV feeder with dedicated transformers (see Fig. 2.3). Such users are characterized by an aggregated peak power consumption of about 300 kW and equipped with 95 kWp of PV rooftop installations. These conditions, along with the large use of power electronics devices, heavily affect the voltage and current profiles, making the EPFL campus a suitable test bed for smart grid experimental activities [5].

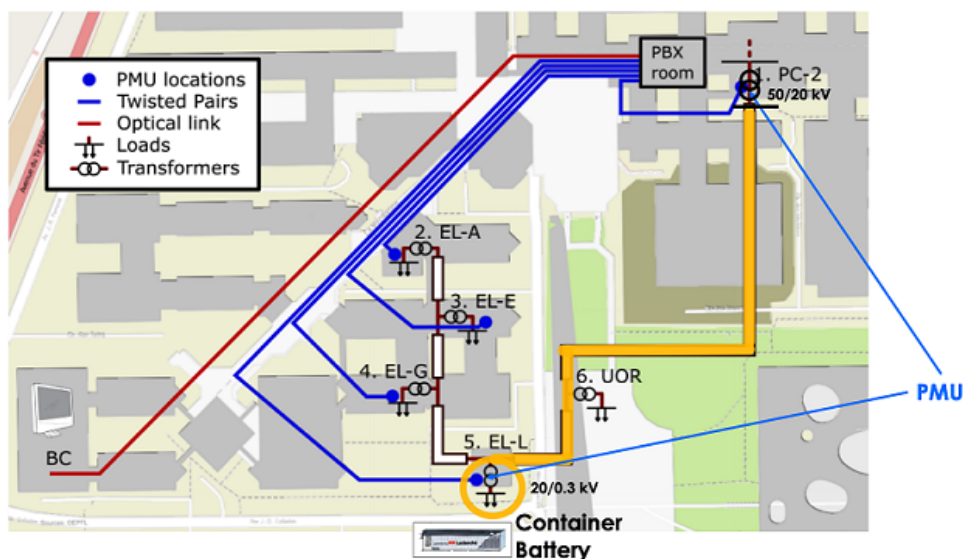


**Figure 2.3:** Topology of the EPFL MV grid under study

The analyzed MV grid is connected to the main 50 kV grid with a 20 MVA 50/20 kV transformer. A 460 m cable connects both transformers to each other. Their parameters are included in Table 2.1.

**Table 2.1:** Large-scale BESSs

Parameter	Value
<b>System parameters</b>	
Energy Capacity	560 kWh
Maximum Power	720 kVA
Nominal Active Power	640 kW
<b>Module parameters</b>	
Nominal Capacity	48 Ah
Total Energy	2.2 kWh
Nominal Current	90 A
Nominal Voltage	46 V
Weight	88 kg
Dimension (L × W × H)	550 × 463 × 356 mm
<b>Inverter parameters</b>	
Maximum AC Power	720 kVA
Nominal AC Power	615 kVA
Rated AC grid voltage	0.3 kV, three-phase
Maximum AC current	1385 A
AC current distortion (THD)	3%
Nominal DC voltage	750 V
DC voltage range	500-890 V
Efficiency	≥97%
<b>Step-up Transformer parameters</b>	
Rated power	630 kVA
High voltage	3 x 20 kV
Low voltage	3 x 0.3 kV
Short circuit voltage	6%
Group	Dd0
<b>EPFL grid Transformer parameters</b>	
Rated power	20 MVA
High voltage	3 x 50 kV
Low voltage	3 x 20 kV
Short circuit voltage	9%
Group	Ynd11

In addition, the MV grid has been completely instrumented with a widespread real-time PMU-based monitoring infrastructure, which locations are depicted in Fig. 2.3. In this project, 2 PMU will be used: the one at the 20 kV bus of the battery transformer and the one at the 50 kV side of the main transformer.

## 2.1.2 Communication protocols

The industrial controllers implementing the control algorithms can communicate with the BESS converter either via *Modbus/TCP* or via *EtherCAT* (read only) serial communications protocol with time steps of 200 ms and 10 ms, respectively.

The set-up and communication system of the master controller (for all strings of battery modules) for large BESS is shown in Fig. 2.4. The communication protocol relies on *Modbus/TCP*.

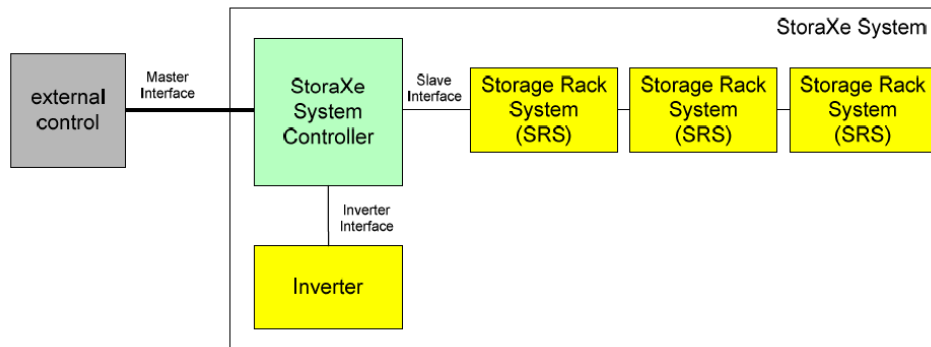


**Figure 2.4:** Master Controller of the large-scale BESS

The set-up and communication system of the slave controller (for each string of battery modules) for the large-scale BESS is shown in Fig. 2.5. The communication protocol relies on *Modbus TCP*.

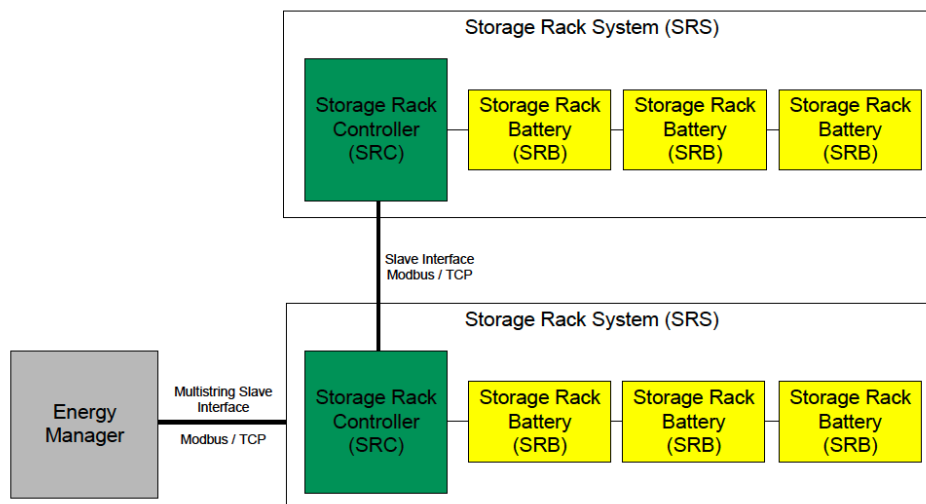


**Figure 2.5:** Slave Controller of the large-scale BESS

There are two ways to communicate (through *Modbus*) with the the BESS and converter:

- Communicate through the master controller (SRC1) with the large-scale BESS and converter together. This is shown in Fig. 2.6a.
- Communicate through the slave controller (SRC2) with the large-scale BESS (strings of battery modules), and with the converter separately. This is shown in Fig. 2.6b. In this setting, the coordination of controls between battery and converter must be guaranteed by the developer of the BESS control strategy.

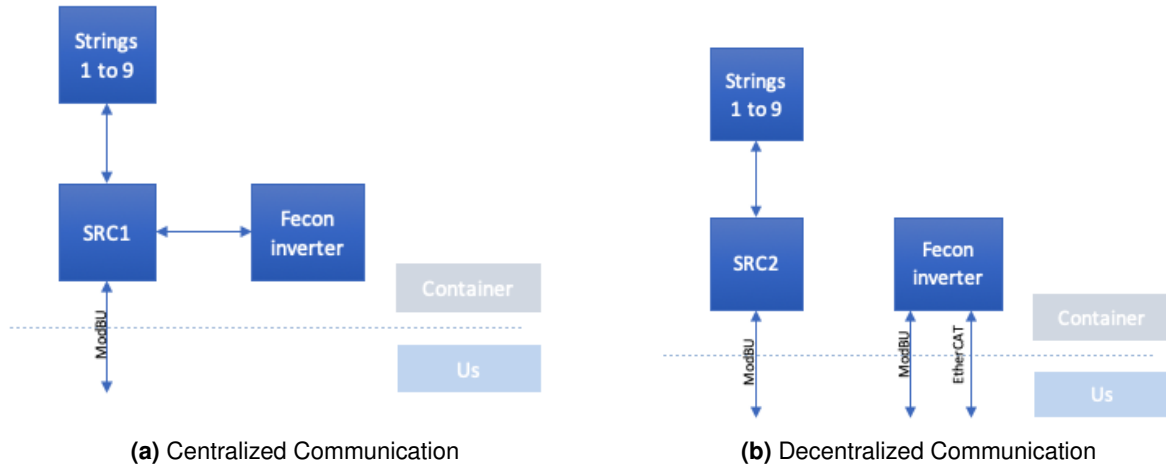


**Figure 2.6:** Communication with the the BESS and converter

## 2.2 Technical description of the small-scale BESS demonstrator

Another possible testbed within the EPFL laboratories is a smaller-scale solution, equivalent to one string of the above-described utility-scale BESS: a LTO battery with 25 kWh capacity. The BESS is connected to a low voltage (LV) experimental microgrid at 400 V through a 25 kW 4-quadrant converter, capable of operating in CSC and VSC control mode. The main circuit of the small-scale BESS is shown in Fig. 2.7, while Table 2.2 summarizes its parameters.

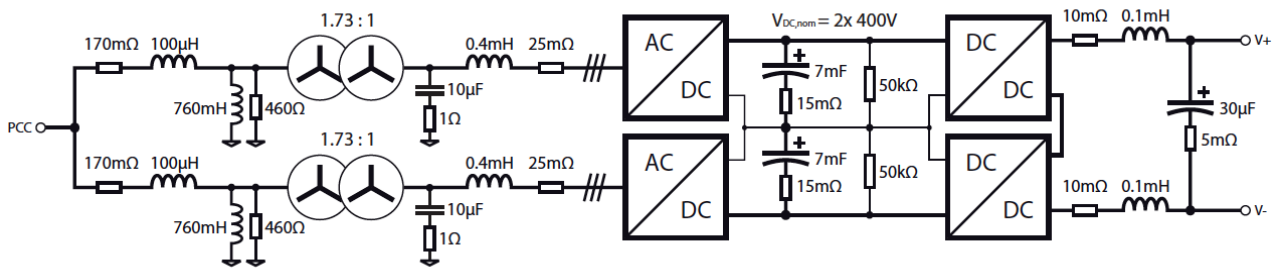


**Figure 2.7:** The main circuit of the small-scale BESS

Provided that the inner control loop can be coded, the grid-forming controller can be implemented. Furthermore, the flexibility of the mentioned control mode enables the experimental validation of simultaneous ancillary services.

### 2.2.1 EPFL LV grid description

The smaller size BESS is part of the EPFL experimental LV microgrid represented in Fig. 2.8. It is a real full-scale representation of the Cigré LV grid benchmark at 400 V [6], and is connected to the external 20 kV MV grid via a 630 kVA 3-phase MV/LV transformer. A diversity of typical distributed energy resource units is present and can be connected at the 400 V cables, and dedicated PMUs are installed at each connection bus. For the small-scale grid-forming tests a radial configuration of the microgrid is considered, which employs three segments of cable in series (total length: 135 m) to connect the battery bus to the MV/LV transformer. In this project 2 PMU measurements will be used: the one at the point of common coupling and the one at the MV side of the LV/MV transformer.

**Table 2.2:** Small-scale BESSs

Parameter	Value
<b>System parameters</b>	
Energy Capacity	28.6 kWh (13 modules)
Maximum Power	53.8 kW
Nominal Power	25 kW
<b>Module parameters</b>	
Nominal Capacity	48 Ah
Total Energy	2.2 kWh
Nominal Current	90 A
Nominal Voltage	46 V
Weight	88 kg
Dimension (L × W × H)	550 × 463 × 356 mm
<b>Inverter parameters</b>	
Maximum AC Power	50 kVA
Nominal AC Power	25 kVA
Rated AC grid voltage	0.4 kV, three-phase
Maximum AC current	72 A
AC current distortion (THD)	3%
Nominal DC voltage	800 V
DC voltage range	440-700 V
Efficiency	≥91%
<b>Converter insulation Transformer parameters</b>	
Rated power	25 kVA (2 units)
High voltage	3 x 0.4 kV
Low voltage	3 x 0.23 kV
Short circuit voltage	3.1%
Group	Yyn0
<b>Microgrid Transformer parameters</b>	
Rated power	630 kVA
High voltage	3 x 20 kV
Low voltage	3 x 0.4 kV
Short circuit voltage	4.4%
Group	Dyn11

### 2.2.2 Communication protocols

The industrial controllers implementing the control algorithms can communicate with the converter via *CAN bus* serial communication protocol with time steps of 50 ms. The hardware setup is shown in Fig. 2.9. The controller of the small-scale BESS is executed in a *National Instruments cRIO 9068*, where all operational loops run:

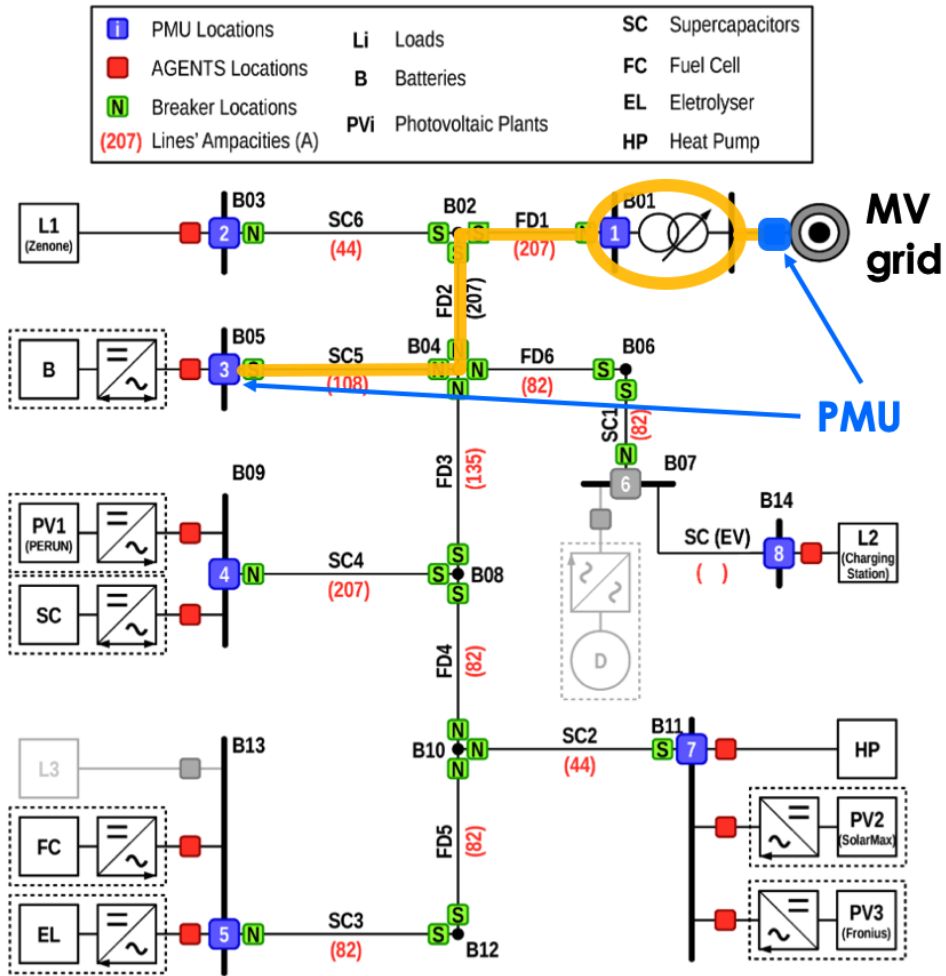


Figure 2.8: Topology of the EPFL experimental LV microgrid

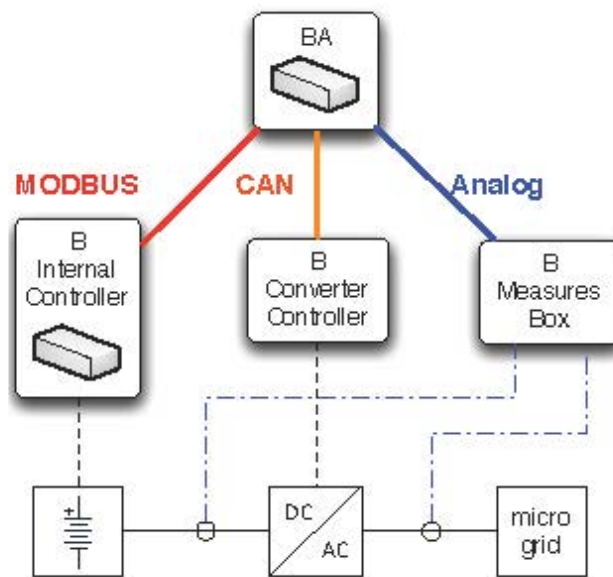
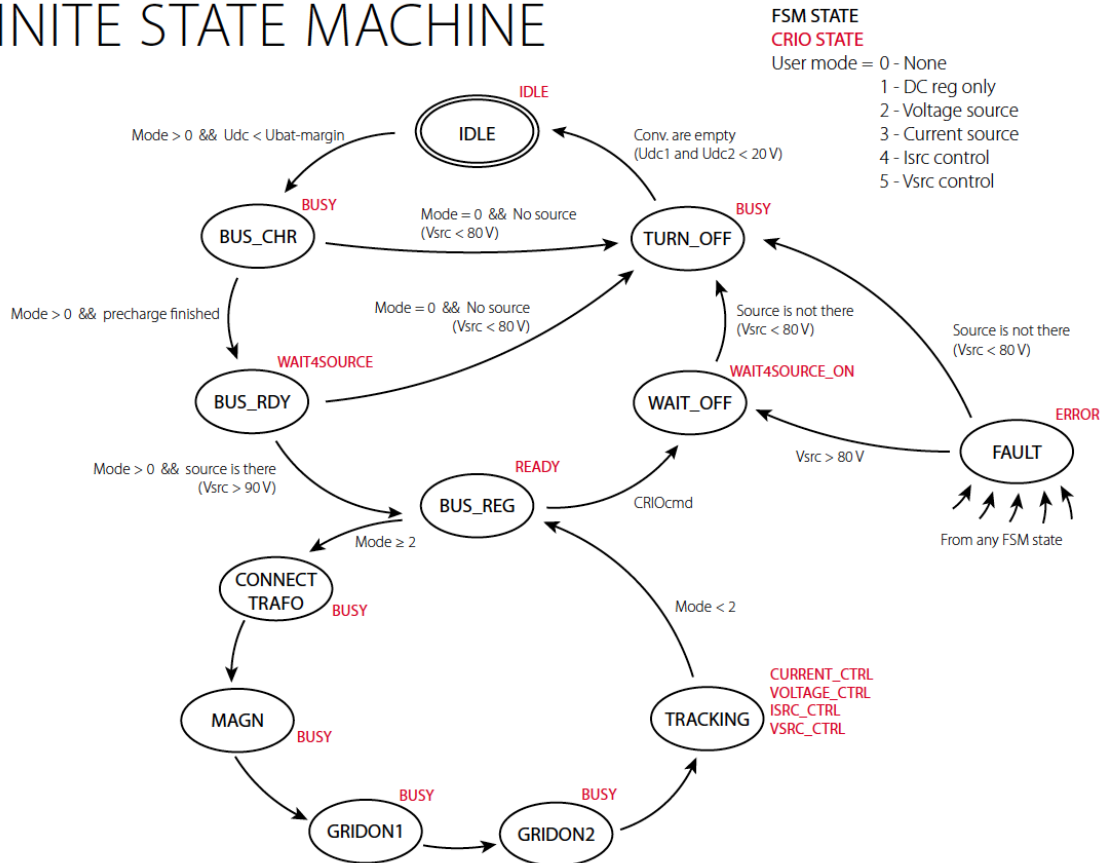


Figure 2.9: Hardware setup of the small-scale BESS control

- DC and AC measurements (using the embedded FPGA);
- CAN communication with the power converter;
- Modbus communication with the BMS (battery management system or internal controller);
- Data logging;
- Operational Finite State-Machine (FSM) shown in Fig. 2.10;
- Battery Agent.

## FINITE STATE MACHINE



**Figure 2.10:** The finite state machine diagram of small BESS converter control

### 2.3 Common data logging infrastructure

For the experimental demonstration activities at EPFL, a throughout data logging infrastructure is employed. Dedicated *p-class* PMUs are available to perform synchronized phase measurements with the technical specifications shown in Fig. 2.11.

Indeed, synchronized PMUs enable the acquisition of real time synchrophasors that can be used to assess the electrical system frequency behavior after a disturbance, thus to assess the effectiveness of the implemented grid-forming controller in the two proposed testbeds. The technology of the adopted PMUs has been developed within the framework of research and development activities at the Distributed Electrical Systems Laboratory (DESL) premises at EPFL. They are FPGA-based *p-class* PMU, rely on a *National Instruments cRIO* platform, and provide a synchrophasor estimation via an Enhanced Interpolated-DFT algorithm with a reporting time of 20 ms [7].

- Synchrophasor Estimation → Enhanced Interpolated-DFT [\*]
- Total Vector Error (TVE) ~ 0.0X %
- Frequency Error < 0.4 mHz
- Reporting Rate 50 frames per second (fps) → Reporting time 20 ms
- GPS Time synchronization → 100 ns accuracy



**Figure 2.11:** The adopted DESL-EPFL PMU

A dedicated server developed within a Debian operating system and located at the DESL premises collects the real time phase measurements. The measurements are stored in the time-series database *InfluxDB* with the reporting time of 20 ms. To allow continuous visualization and monitoring of the acquired measurements, the open source software *Grafana* for data visualization is employed. For each PMU, individual phase voltages, currents (hence power is calculated), frequency and RoCoF measurements can be monitored, allowing a comprehensive overview of the overall status of both the battery and the power grid, and eventually enabling real time calculations for the whole grid state estimation and/or for the implementation of control actions.

A screenshot of the outlook of the *Grafana* monitoring interface is shown in Fig. 2.12. This example reports measurements of the utility-scale BESS active power and the system frequency when a primary frequency controller is implemented to provide grid support. An estimation of the state of charge of the employed BESS is also included, since it is a parameter of utmost importance when managing the charging/discharging process of a battery performing power system regulation.

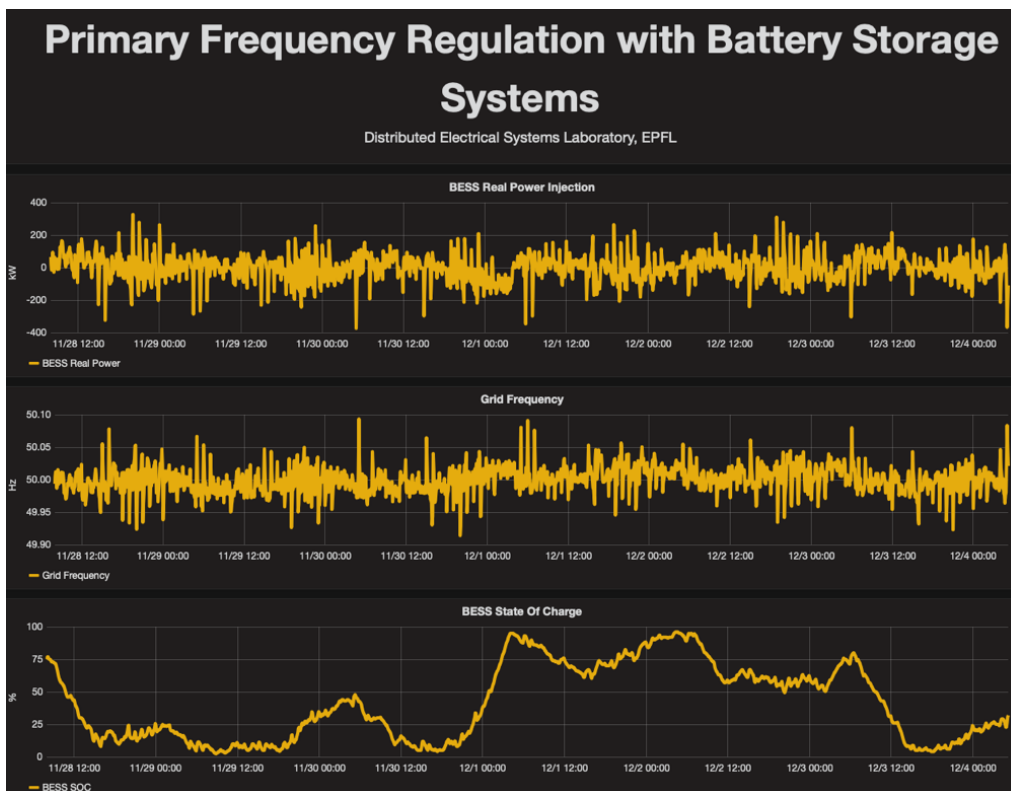


**Figure 2.12:** Screenshot of the outlook of the *Grafana* monitoring interface employed for frequency regulation services via the utility-scale BESS at EPFL

---

## 2.4 Services, tests and performance metrics

Although the main objective of the demonstration is the implementation on real hardware of the grid-forming controller, other services will be tested in the two selected test-beds, namely the utility-scale BESS and the small-scale setups. Indeed, they both enable the implementation of the grid-forming controller as well as of the controllers for other grid services, such as:

- The first ancillary service that can be implemented and validated is **frequency control**. During frequency variations originated by power unbalances, the utility-scale and the small-scale BESS can be controlled to provide primary reserve to the system.
- Multiple services including **primary frequency response**, **dispatch** and **voltage control** can also be clustered in both setups.
- The small-scale BESS can be tested in **is-landing** mode of a micro-grid setup.

As described above, in both setups measurements are acquired via *P-class* PMUs, which enable a comprehensive assessment of the effectiveness of the BESS contribution in the different test cases.

In the large-scale grid forming BESS setup, the measurements of two PMUs (one close to the battery and one at the HV side of the EPFL grid transformer) are compared when a load variation is triggered. It is expected that the variation in the measurement is at least 10 times larger than the accuracy of the acquired PMU measurement, which is 0.4 mHz.

In this case, the probability density function (*PDF*) of both frequency or voltage measurements, defined as  $metric_1$ , can provide insights on the actual influence of the controller on the (local) system frequency measured at the grid connection point. Then, a comparison of the *PDF* when the different service are enabled or not will allow to assess the impact of the services.

$$PDF_{\Delta f(\Delta v)} = \frac{\text{Number of measurement samples in given frequency range } \Delta f(\Delta v)}{\text{Total number of measurement samples of frequency } f(\text{or voltage } v)} \quad (2.1)$$

In the small-scale BESS setup, PMUs measurements are available at the LV grid connection point and at the MV side of the microgrid transformer. Also in this setup, it is expected that the variation in the measurement is at least 10 times larger than the accuracy of the acquired PMU measurement, which is 0.4 mHz. Similar analysis of the frequency and voltage measurements as in the large-scale BESS can be performed ( $metric_1$ ).

Furthermore, as the system can run also in islanded mode, a load contingency can be used to destabilize the microgrid frequency. In this case, both the lowest value of the frequency (nadir) and the rate of change of frequency (RoCoF) can be used as the performance metrics when the grid-forming controller is implemented in the BESS.

Therefore,  $metric_2 = Max(RoCoF)$ ,  $metric_3 = Nadir$  can be used for frequency smoothing performance <sup>1</sup> and  $metric_4 = \Delta(V)$  the voltage amplitude drop/increase after load contingency can be deployed here to evaluate the voltage smoothing performance.

---

<sup>1</sup>There are multiple ways to measure frequency, and especially during transient, the different ways or measurement can lead to different results. The aim of this project is not to go into details in frequency measurement. Therefore, to have a fair comparison, only one type of frequency measurement will be used for all tests and on the different demos. The type-P PMU developed by EPFL [8] will be used.

## 2.5 39-bus power system model for real time simulation

To study the impact of inertia reduction on system frequency dynamics, two IEEE 39-bus dynamic power system configurations are compared (see Fig. 2.13). Figure 2.13a shows the original IEEE 39-bus power system with 10 synchronous generations (noted as Config. I). Figure 2.13b presents an "inertia-reduced" 39-bus power system (noted as Config. II), where 4 synchronous generations (i.e. G1, G5, G8, and G9) are replaced by 4 wind plants (i.e. WP1, WP2, WP3 and WP4). As a summary, Table 2.3 reports the plant type, nominal capacity and frequency regulation for each generator, and the modelling details are given in this section.

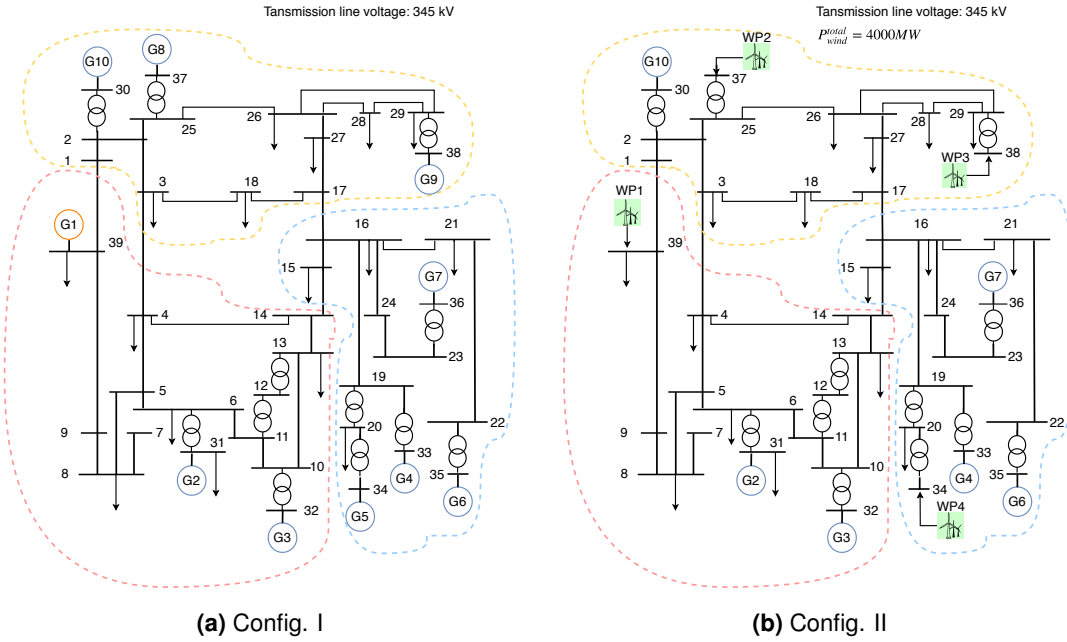


**Figure 2.13:** Diagrams of IEEE 39-bus dynamic power systems

### 2.5.1 Main component models

#### 2.5.1.1 Synchronous Generators

The conventional generation park consists of both hydro- and thermal-power plants that are simulated by means of a six-order state-space model for the synchronous machine, a prime mover [9], a speed governor [10], a DC1A excitation system and an AVR [11].

The model of the steam turbine is based on a complete tandem-compound steam prime mover, equipped with a speed governing system, four-stage steam turbine, and four-mass shaft. The speed governing system of the steam turbine is similar to what proposed in [10]. It consists in a speed governor, speed delay, hydraulic servomotor and governor-controlled valves. The speed-governing system is shown in Fig. 2.14. The speed reference (SR) signal is set to a constant value as in this work we do not implement automatic generation control; the speed governor is represented by a gain  $K_G$  which is the reciprocal of primary frequency droop coefficient; the speed delay is represented by an integrator with time constant  $T_{SR} = 0.001$ ; the hydraulic servomotor is modelled with an integrator with time constant  $T_{SM} = 0.15$  and  $\dot{C}_{vopen} = 0.1$  and  $\dot{C}_{vclose} = -0.1$  as servomotor's speed maximum and minimum limits; the speed of the servomotor is integrated to obtain the position, the maximum and minimum limits of which are  $C_{vmax} = 4.496$  and  $C_{vmin} = 0$ . The droop coefficient of all the conventional generators is 5%, i.e.  $K_G = 20$  for the steam turbine.

**Table 2.3:** List of Generation Units

Generation Unit	Plant Type	Installed Capacity [MVA]	Inertia Constant H [s]	Frequency regulation	Location
G1	Thermal Plant	3000	16.7	PFC	39
G2		1000	3.03	PFC	31
G3		1000	3.58	PFC	32
G4		1000	2.86	PFC	33
G5		520	5.2	PFC	34
G6	Hydro Plant	1000	3.48	PFC	35
G7		1000	2.64	PFC,SFC	36
G8		1000	2.43	PFC	37
G9		1000	3.45	PFC	38
G10		1000	4.2	PFC	30
WP1		1600	-	-	39
WP2	Type-3 DFIG	1300	-	-	37
WP3		900	-	-	38
WP4		700	-	-	34

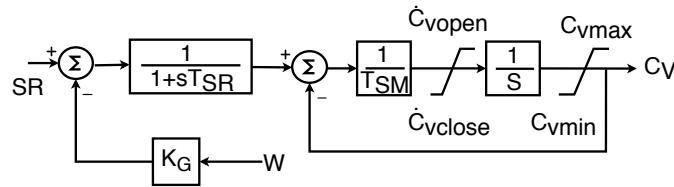


**Figure 2.14:** Diagram of the speed-governing system of the steam turbines.

The model of the hydro power plant consists of a non-linear hydraulic turbine model and the associated speed-governing system, which is a servomotor controlled by a PID regulator. The hydraulic turbine model is a non-linear model from the Simulink SimPowerSystem library. The modeling of the hydro turbine's speed-governing system is based on [12]. Figure 2.15 shows the speed governor that generates the gate opening signal for the hydraulic turbine. The servomotor is modelled by the first-order system, where  $K_a = 3.33$  and  $T_a = 0.07$  are the gain and time constant. This model uses the electrical power deviation as droop reference, passing the control signal to a PID controller. The static gain of the governor is equal to the inverse of the permanent droop  $R_p$  in the feedback loop. The droop coefficient for all hydro power generation units is 5%.

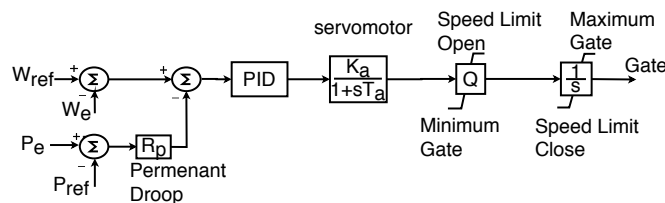


**Figure 2.15:** Model of the speed governor of hydro turbine.

Figure 2.16 shows the diagram of the excitation system. The  $V_{ref}$ ,  $V_g$  and  $V_{f0}$  signals are respectively the reference voltage, measured positive sequence voltage and initial field voltage of the generator. Here  $k_e=1$ . The compared signal is sent to the AVR, that is represented by a first-order transfer function with a saturation block.

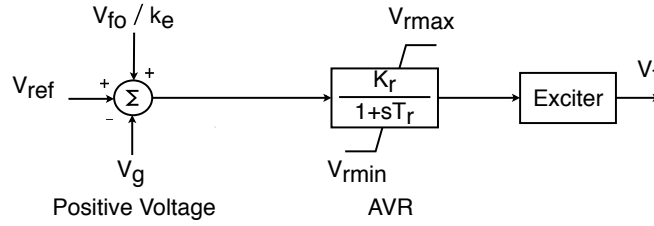


**Figure 2.16:** The IEEE DC1A excitation system.

The parameters are  $k_r = 200$ ,  $T_r = 0.001$ ,  $V_{rmin} = 0$  and  $V_{rmax} = 12.3$  (p.u.) for steam generators, and  $k_r = 200$ ,  $T_r = 0.02$ ,  $V_{rmin} = 0$  and  $V_{rmax} = 7.32$  (p.u.) for hydro generators.

### 2.5.1.2 Dynamic Loads

In order to reproduce a plausible dynamic load behavior, the EPRI LOADSYN model has been adopted [13]. Specifically, the load response to voltage and frequency variations is modeled according to the following:

$$P(t) = P_0(t) \left( \frac{V(t)}{V_0} \right)^{K_{pv}} [1 + K_{pf}(f(t) - f_0)]$$

$$Q(t) = Q_0(t) \left( \frac{V(t)}{V_0} \right)^{K_{qv}} [1 + K_{qf}(f(t) - f_0)]$$

where  $P(t)$  and  $Q(t)$  are the total three-phase load active and reactive power.

The parameters  $K_{pv}$ ,  $K_{pf}$ ,  $K_{qv}$ ,  $K_{qf}$  are obtained from typical load voltage and frequency parameters inferred from EPRI LOADSYN program [13]. In this regard, we represent  $f(t)$ ,  $V(t)$ ,  $P_0(t)$ , and  $Q_0(t)$  as time-varying variables sampled with a resolution of 20 ms.

The voltage waveform used to feed the dynamic load model is the one at phase "a". We assume that  $P_0(t)$  and  $Q_0(t)$  are active and reactive power profiles at rated frequency and voltage. These rated demand profiles are sampled from a monitoring system based on PMUs installed on the 125 kV sub-transmission system of Lausanne, Switzerland [14].

Coherently with the other model variables, the measured time-series power data are sampled with a resolution of 20 ms. Since the nominal load values in the original IEEE 39-Bus power system are different from our measured data, the implemented time series used to produce  $P_0(t)$  and  $Q_0(t)$  are obtained by re-scaling the measured time series.

The implementation of the EPRI LOADSYN model is illustrated in Fig. 2.17. A Phase Lock Loop (PLL) and a Root Mean Squate (RMS) operator measure the bus frequency and voltage feeding the dynamic load model. In order to smooth the response of the PLL in transient conditions, a moving average operator is implemented. Specifically, the PLL-tracked frequency is updated every 1 ms, and then buffered for averaging. The overall buffer size is 240 samples, with an overlap size of 220 samples (i.e., the final frequency  $f(t)$  is reported every 20 ms).

On the other side, the bus voltage  $V(t)$  is given by a RMS operator reporting every 20 ms. The RMS value is computed over a window length of 240 ms, as to be consistent with the frequency estimation.

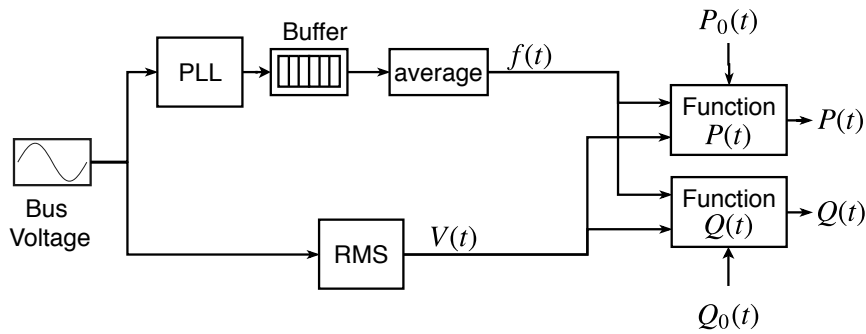


**Figure 2.17:** Diagram of the EPRI LOADSYN dynamic load model.

### 2.5.1.3 Transmission Lines and Transformers

The transmission line model is a ARTEMiS distributed parameter line with lumped losses [15]. The model is based on Bergeron's travelling wave method used by EMTP [16]. The ARTEMiS distributed parameters line block is optimized for discrete real-time simulation and allows network decoupling. Three-phase transformers are modeled via suitably-connected single-phase transformers, which take in account the winding resistances and leakage inductance, as well as the magnetizing characteristics of the core modeled by a linear branch.

When the 4 synchronous generations are replaced by 4 wind plants, their transformers are also adapted correspondingly.

### 2.5.1.4 Wind Power Plants

Each wind power plant is modeled as proposed in [17]. It is approximated by multiplying the power output of a detailed model of a single wind turbine to match the total nominal capacity of the whole wind farm. The diagram of the overall system is shown in Fig. 2.18. The model of each wind generator consists of a DFIG and an averaged back-to-back converter model from [18].

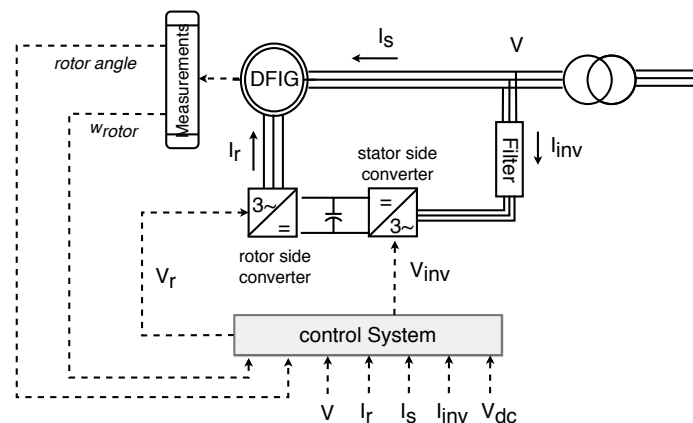


**Figure 2.18:** Diagram of the wind plant's model

The back-to-back IGBT VSCs are modelled by equivalent voltage sources, which generate the AC voltage averaged over one cycle of the switching frequency. In this averaged model, the dynamics resulting from the interaction between the control system and the power system is preserved. Two grid-feeding controls are implemented in the back-to-back converters, as shown in Fig. 2.19.

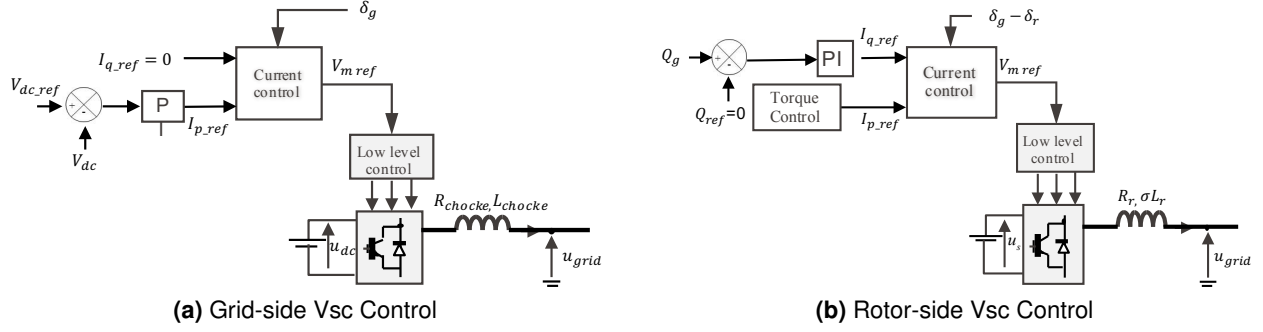


**Figure 2.19:** Diagrams of back-to-back converter controllers used in the type-3 wind turbine model

The detailed aerodynamic model of the wind turbine is neglected as the available data directly refers to power inputs into the DFIG provided by the wind turbine. Indeed, the wind power profiles are generated at 1 second resolution by re-sampling the available measurements at 1 minute resolution from ERCOT [19]. The re-sampling approach is based on iterated smoothing and differentiating operations that use the statistical characteristics of the aggregated wind generation profiles presented in [20] and summarized in the following for the sake of clarity:

Let  $x_t$ ,  $t = 1, \dots, T$  denote a time sequence of  $T$  aggregated wind power generation values at 1 minute resolution, in per unit. We define a new higher resolution sequence  $w_{ts}^b$  for  $t = 1, \dots, T$ ,  $s = 1, \dots, 60$ , at each bus  $b$  of the system where wind farms are connected. In other words,  $w_{ts}^b$  is an over sampled version of  $x_t$  to be obtained using the following process. The differentiated time series of  $w_{ts}^b$ , is denoted by  $\Delta w_{ts}^b$  and computed as:

$$\Delta w_{ts}^b = w_{t,s+1}^b - w_{ts}^b, \text{ for } t = 1, \dots, T, s = 1, \dots, 60. \quad (2.2)$$

During each 1 minute time interval  $t$ , the components of the differentiated time series,  $\Delta w_{ts}^b$ ,  $s = 1, \dots, 60$ , are sampled from a Gaussian distribution  $\mathcal{N}(\bar{w}_t, \sigma^2)$ , where  $\bar{w}_t = (x_{t+1} - x_t)/60$  is the average slope of the original wind generation profile, and  $\sigma^2$  is estimated based on the statistical characteristics of the aggregated wind generation profiles presented in [20].

Finally, the synthetic profile of wind power generation at 1 second resolution in per unit is:

$$w_{ts}^b = x_t + \sum_{s'=1}^s \Delta w_{ts'}^b. \quad (2.3)$$

The power generation profile for an aggregated wind farm connected at bus  $b$  is:

$$W_{ts}^b = W^b \cdot w_{ts}^b, \quad (2.4)$$

where  $W^b$  is the forecast power of the wind farm.

## 2.5.2 BESS-VSC model

In order to study the impact of BESS-VSC on the dynamics of the "inertia-reduced" power system, a BESS-VSC is added to bus 27 in Config. II, referring to Fig. 2.20. Figure. 2.21 presents a simplified diagram of BESS-VSC. Here, the models used to represent its components are detailed.

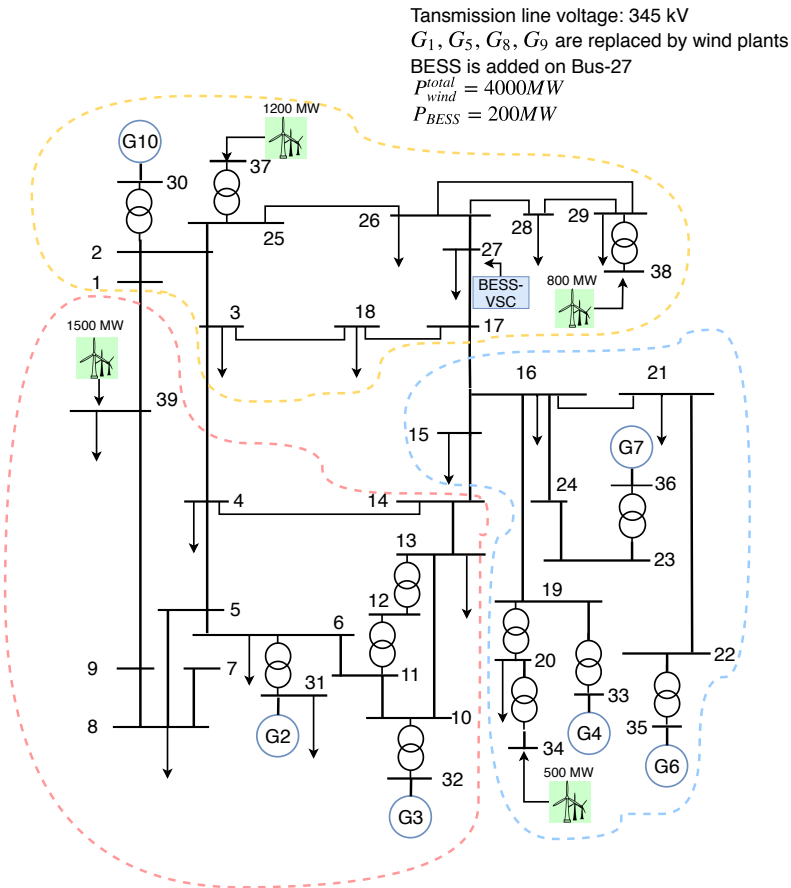


**Figure 2.20:** A BESS integrated into power system Config. II

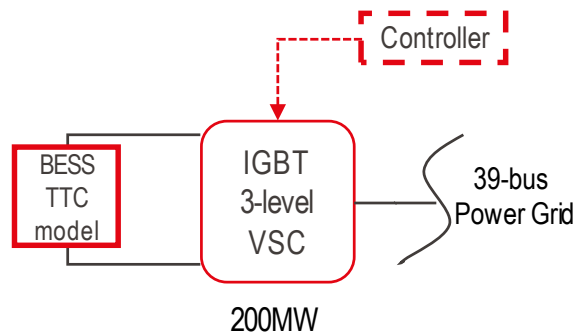


**Figure 2.21:** Diagram of BESS-VSC

### 2.5.2.1 Grid-forming control

A grid-forming control generally refers to the diagram shown in Fig. 2.22. The implemented grid-forming control (see Fig. 2.23) is adapted from the MIGRATE project [21]. Such control creates a link between the inverter output voltage angle and the active power, hence resembling a synchronising torque on the inverter voltage angle. As a result, the power-frequency droop control is coupled with the synchronization control. It is worth noting that this scheme does not need any frequency measurement by PLL to reach an unique synchronization frequency at steady state.

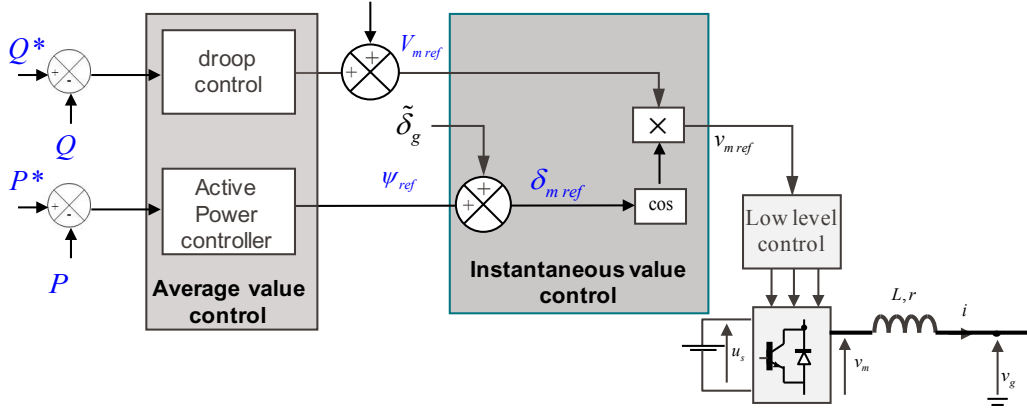


Figure 2.22: Diagram of grid-forming control

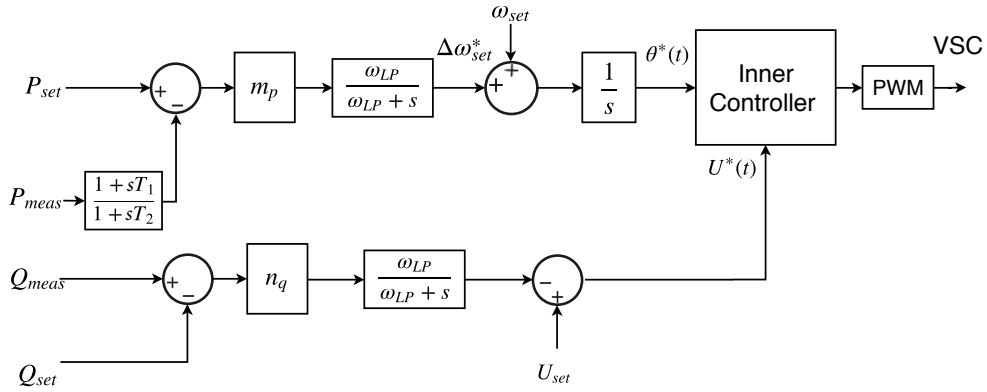


Figure 2.23: Diagram of VSC control from MIGRATE

### 2.5.2.2 Grid-feeding control

A grid-feeding control generally refers to the diagram shown in Fig. 2.24. The implemented grid-feeding control (see Fig. 2.25) is embedded with an external frequency control to provide power grid frequency regulation services. The PLL is used to estimate the grid voltage angle so that the active power and reactive power can be controlled independently via controlling the direct and quadrature currents.

### 2.5.2.3 BESS TTC model

Figure. 2.26 shows the equivalent circuit of a TTC model, whereby can be implemented into Simulink as a state space model (SSM):

$$\frac{dx(t)}{dt} = A_c(SOC)x(t) + B_c(SOC)u(t)$$

$$y(t) = C_c(SOC)x(t) + D_c(SOC)u(t)$$

$$\text{where, } A_c = \begin{bmatrix} -\frac{1}{R_1 C_1} & 0 & 0 \\ 0 & -\frac{1}{R_2 C_2} & 0 \\ 0 & 0 & -\frac{1}{R_3 C_3} \end{bmatrix}, B_c = \begin{bmatrix} \frac{1}{C_1} & 0 \\ \frac{1}{C_2} & 0 \\ \frac{1}{C_3} & 0 \end{bmatrix}, C_c = [1 \quad 1 \quad 1], D_c = [R_s \quad E],$$

$$x = [v_{C1} \quad v_{C2} \quad v_{C3}], u(t) = [i_t \quad 1].$$

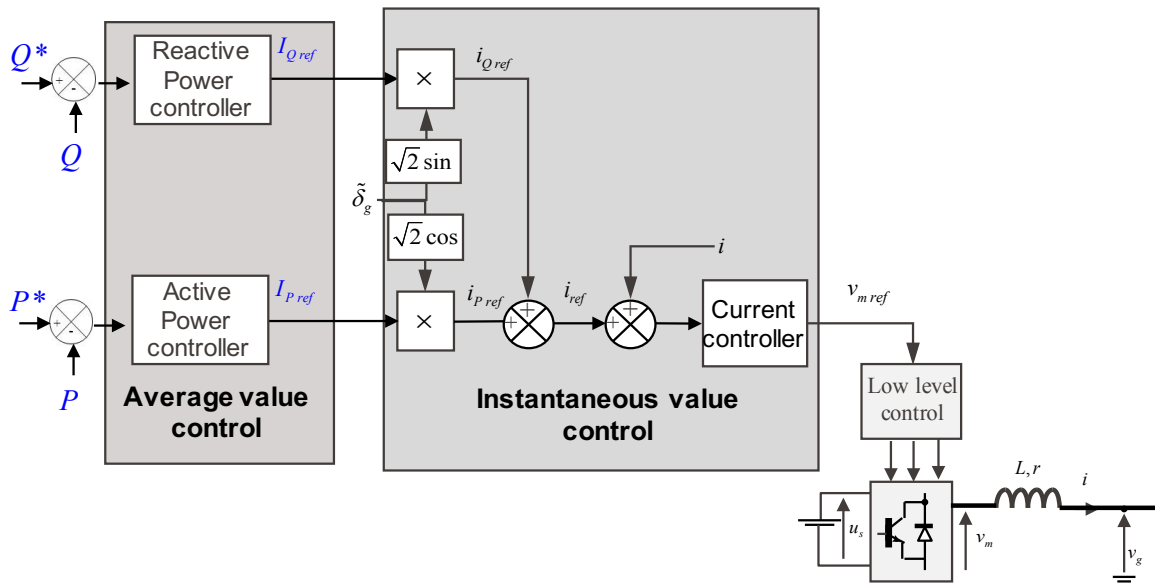


Figure 2.24: Diagram of grid-feeding control

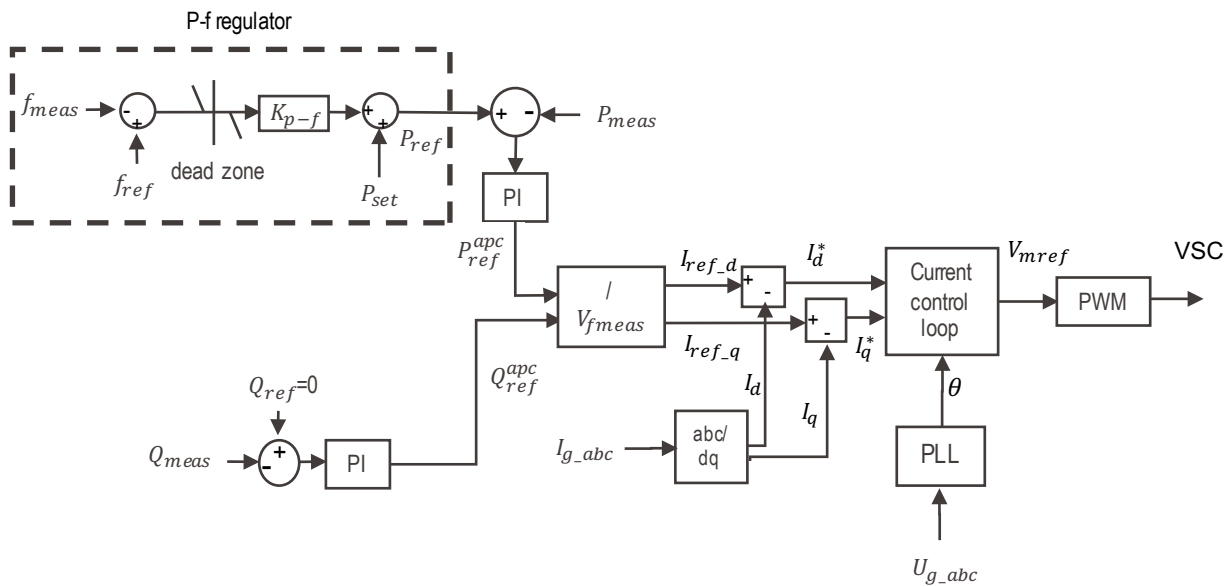


Figure 2.25: Diagram of the adopted grid-feeding control embedding outer loop control for frequency control

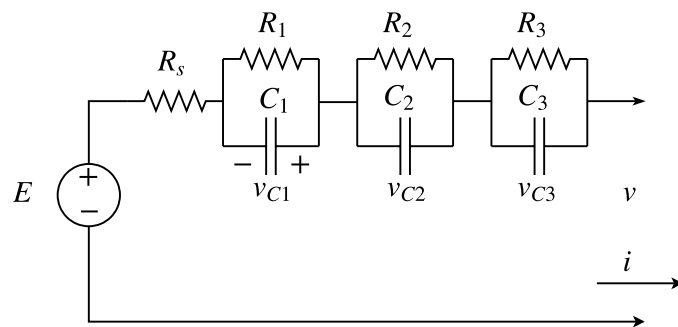


Figure 2.26: Three Time Constant Equivalent Circuit of the BESS

The adopted BESS model (noted as  $BESS_{rts}$ ) is developed on the basis of a TTC model, which parameters are shown in Table 2.4 and have been identified using real data from a 720kVA/560kWh BESS (noted as  $BESS_{desl}$ ) available at the EPFL-DESL [22]. The electrochemistry of the battery is Lithium Titanate Oxide. The nominal active power of  $BESS_{desl}$  is 640 kW, the nominal capacity is 750 (Ah) (ampere-hour) and the nominal DC voltage of connected inverter is 750 V.

**Table 2.4:** Parameters of 560 kWh Lithium Titanate Oxide BESS available at the EPFL-DESL

SOC [%]	0-20	20-40	40-60	60-80	80-100
E	586.2	619	646.9	674.2	727.2
Rs	0.029	0.021	0.015	0.014	0.013
R1	0.095	0.075	0.090	0.079	0.199
C1	8930	9809	13996	12000	11234
R2	0.04	0.009	0.009	0.009	0.10
C2	909	2139	2482	2490	2505
R3	2.5e-3	4.9e-5	2.4e-4	6.8e-4	6.0e-4
C3	544.2	789.0	2959.7	4500	6177.3

Since the nominal active power of the  $BESS_{desl}$  is way lower than the one expected to be connected to a HV transmission grid, the  $BESS_{desl}$  SSM (noted as  $SSM_{desl}$ ) need be scaled-up to obtain a 200 MW  $BESS_{rts}$  SSM (noted as  $SSM_{rts}$ ). To this end, the  $SSM_{rts}$  is realised by connecting in parallel 156 battery packs, where each battery pack consists of two  $SSM_{desl}$  connected in series. Figure 2.27 shows the configuration of the  $SSM_{rts}$ . Assuming that all paralleled battery packs are identical, the parameters for  $SSM_{rts}$  are adapted as shown in Table 2.5.

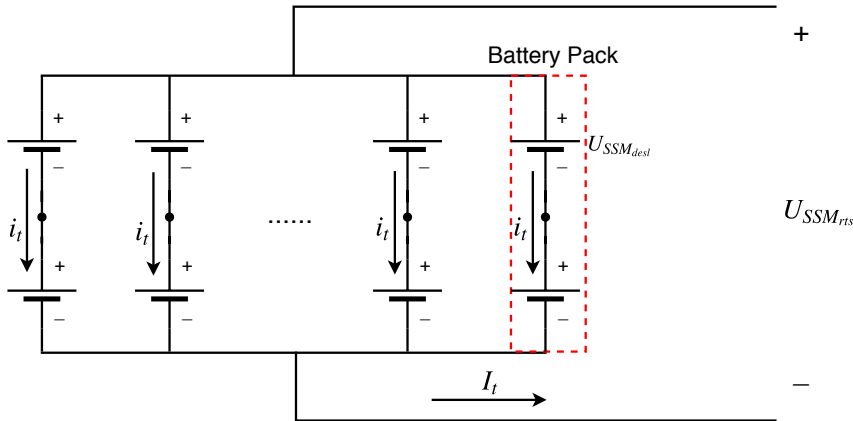


**Figure 2.27:** Configuration of  $SSM_{rts}$

Thereby, the  $SSM_{rts}$  is formulated as:

$$\frac{dx^*(t)}{dt} = A_c^*(SOC)x^*(t) + B_c^*(SOC)u^*(t)$$

$$y^*(t) = C_c^*(SOC)x^*(t) + D_c^*(SOC)u^*(t)$$

$$\text{where, } A_c^* = \begin{bmatrix} -\frac{1}{R_1 C_1} & 0 & 0 \\ 0 & -\frac{1}{R_2 C_2} & 0 \\ 0 & 0 & -\frac{1}{R_3 C_3} \end{bmatrix}, B_c^* = \begin{bmatrix} \frac{1}{C_1} & 0 \\ \frac{1}{C_2} & 0 \\ \frac{1}{C_3} & 0 \end{bmatrix}, C_c^* = \begin{bmatrix} 1 & 1 & 1 \end{bmatrix}, D_c^* = \begin{bmatrix} R_s^* & E^* \end{bmatrix},$$

**Table 2.5:** Parameters of one battery pack of the  $BESS_{rts}$ 

SOC [%]	0-20	20-40	40-60	60-80	80-100
$E^*$	1172.4	1238	1293.8	1348.4	1454.4
$R_s^*$	0.052	0.042	0.030	0.028	0.026
$R1^*$	0.190	0.150	0.180	0.158	0.398
$C1^*$	4465	4904.5	6998	6000	5617
$R2^*$	0.08	0.018	0.018	0.018	0.20
$C2^*$	454.5	1069.5	1241	1245	1252.5
$R3^*$	5.0e-3	9.8e-5	4.8e-4	13.6e-4	12.0e-4
$C3^*$	272.1	394.5	1479.8	2250	3088.7

$$x^* = [v_{C1} \ v_{C2} \ v_{C3}], \ u^*(t) = \left[ \frac{I_t}{156} \ 1 \right], \text{ and } U_{SSM_{rts}} = y^*(t).$$

As the battery pack are formed by two 720kVA/560kWh BESSs connected in series, the maximal power and energy capacity of the battery pack become 1.44 MW and 1.12 MWh, and the nominal DC voltage of the connected inverter is 1.5 kV. Therefore, the adopted  $BESS_{rts}$ , which consists of 156 battery packs connected in parallel, is a 225MVA/176MWh BESS.

Note that the input current of the  $SSM_{rts}$  (first entry of the vector  $u^*(t)$ ) is  $\frac{I_t}{156}$ , where  $I_t$  is the total DC current absorbed/provided by the  $BESS_{rts}$ . As we assume all the battery packs operating identically, an aggregated  $BESS_{rts}$  SOC model is adopted for computing battery SOC according to:

$$SOC_{k+1} = SOC_k + \frac{T_s}{3600} \frac{I_k/156}{C_{nom}}$$

where  $C_{nom} = 750$  (Ah) is BESS capacity denoted in ampere-hour,  $T_s = 0.001$  s is SOC model sampling rate, and  $I_k$  is the total DC current absorbed/provided by the  $BESS_{rts}$ .

#### 2.5.2.4 Three-level NPC converter

The BESS is integrated into the IEEE 39-bus through an aggregated fully modeled three-level neutral-point clamped (NPC) converter. Figure. 2.28 shows the original Simulink model of the 3-level converter, which cannot be directly implemented in the real-time simulation model due to involving two many switch devices in one SSN (state space nodal) group [23]. The proposed solution consists in distributing those switch devices into different SSN groups as show in Fig. 2.29.

The three bridge arms (one arm refers to the red rectangular in Fig. 2.28) of the 3-level converter are respectively included into subsystem "3-level NPC 1", "3-level NPC 2 " and "3-level NPC 3". Each arm interface with AC and DC side through two ARTMiS-SSN interface blocks that are used to define nodes and groups of SSN solver. The parameters for electrical elements on DC-side, AC-side and IGBT/Diodes pairs are listed on Table 2.6.

**Table 2.6:** Parameters for VSC

DC			AC		IGBT/Diodes
$R_{sr} \ L_{sr}$ [ $\Omega$ ] [htbp]	$R_{dcf} \ C_{dcf} \ L_{dcf}$ [ $\Omega$ ] [ $\mu$ F] [htbp]	$C_{dc}$ [ $\mu$ F]	$R_r \ L_r$ [ $\Omega$ ] [htbp]	$[f_{T1} \ f_{T2}] [Q_{f1} \ Q_{f2}]$ [kHz] [Mvar]	$R_{on} \ R_{snu} \ C_{snu}$ [m $\Omega$ ] [ $\Omega$ ] [ $\mu$ F]
0.0251 0.087	0.14737 12 0.0469	70	0.015 0.0048	[1.35 2.7] [18 22]	0.1 2000 Inf

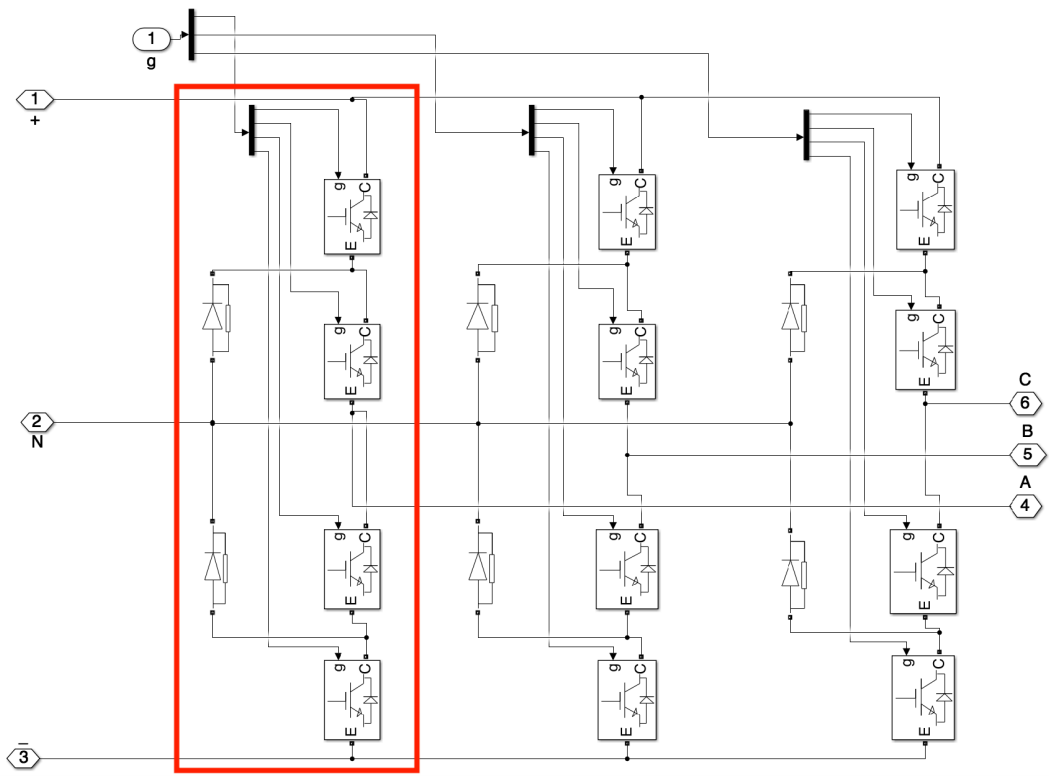


**Figure 2.28:** IGBT-based three-level NPC converter

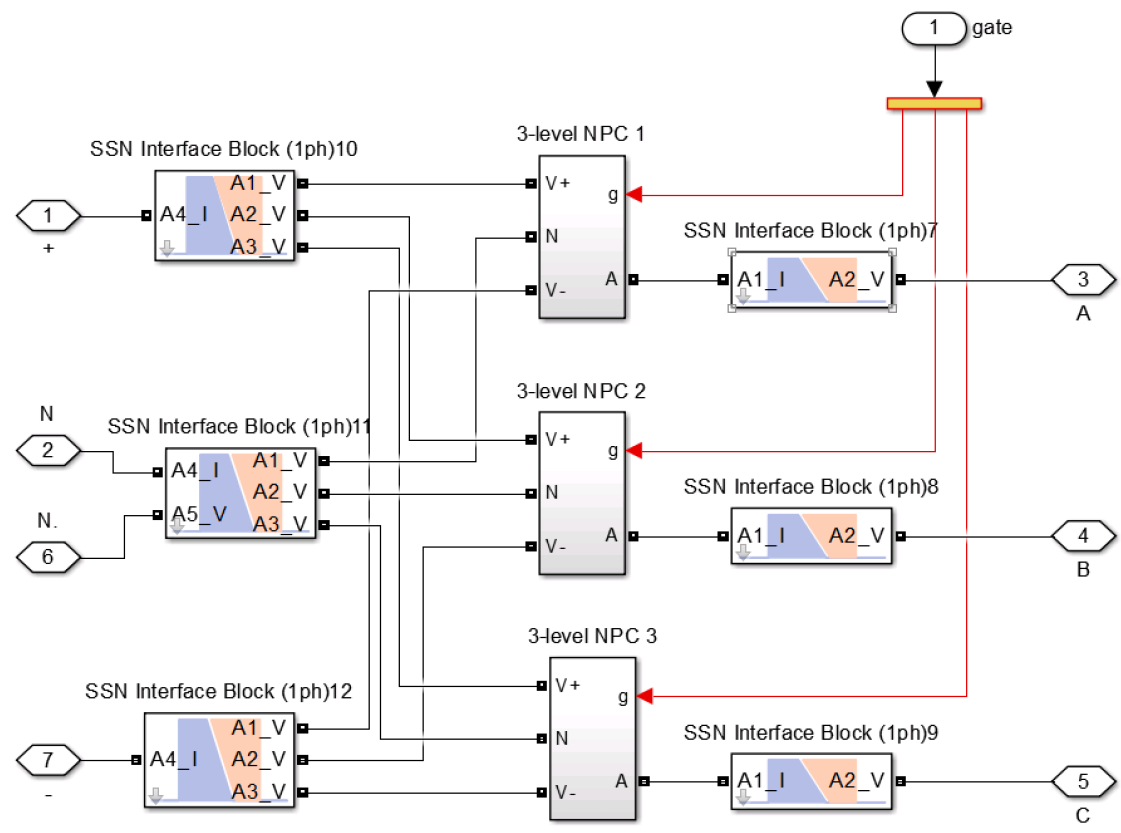


**Figure 2.29:** IGBT-based three-level NPC converter model in RT simulation

---

### 2.5.3 Data logging infrastructure

Concerning the 39-bus power system real-time simulations, MATLAB/Simulink and RT-LAB are required. The 39-bus power system models are built in MATLAB/Simulink and RT-LAB is a distributed real-time platform that enables the Simulink models to be executed on the OPAL-RT real-time simulators. The real-time simulator used for this report is OPAL-RT OP5600 installed with the corresponding RT-LAB version v11.2.2.108 and ARTEMIS Block-set version 7.2.2.1206.

To execute the 39-bus power system models for real-time simulation at the fix time step of  $25 \mu s$ , at least 7 cores should be available in the OP5600 simulator. The software version of a realistic *P-class* PMU [8] can be used to obtain voltage, frequency and ROCOF measurements.

In terms of data logging in real-time simulation, we use "OpWriteFile" block provided by RT-LAB to save data a MATLAB file format (.m) without interfering with real-time simulation.

### 2.5.4 Test events and performance metrics for the real-time simulation

A realistic model of the *class P/M* PMU compliant with the technique standard IEEE C37.118.1a-2014 on EPFL campus is implemented in the 39-bus grid simulation model. This enables realistic acquirement of measurements of frequencies and voltages. The proposed test events and corresponding key performance indicators (KPIs) are listed in the following.

- **Tripping of synchronous generation:** the KPIs are proposed as follows:

For comparing Config. I with Config. II, the KPIs are system RoCoF and frequency Nadir evaluating the impact of inertia reduction ( $metric_2$  and  $metric_3$ ).

For comparing the grid-forming control to the grid-feeding control, the analyzed KPIs focus on system RoCoF, frequency Nadir, ( $metric_2$  and  $metric_3$ ) and battery power output smoothing ( $metric_5$ ) given by the derivative of the power output.

$$metric_5 = \frac{\Delta P_{Bat}}{dt} \frac{1}{Pn_{Bat}}$$

The aim is to see how much stress is put on the battery with the different controls.

- **Multi-services with respect to frequency response services**

A long period of real-time simulation will be conducted for the "reduced inertia" power system with a BESS-VSC connected. The frequency response services will be quantified as the reduction of primary, secondary and tertiary frequency reserve ( $metric_6$ ). Furthermore we can also use  $metric_6$  and  $metric_1$  to evaluate the performance.

$$metric_6 = \frac{Scheduled Reserve - Activated Reserve}{Scheduled Reserve} \quad (2.5)$$

- **Is-landing test**

A regional power grid, which includes the BESS-VSC but without synchronous generation will be isolated caused by disconnection of transmission lines. Thereby, this isolated power grid is expected to operate in is-landing mode.

The objective is to compare the grid-forming control with grid-feeding control in the aspect of keeping stability under is-landing operation ( $metric_1, metric_2, metric_3, metric_4$ ).

## 3 RingoLab Demo (RTE/Ingeteam)

### 3.1 Presentation of Ringolab Overall specification

The Ringolab will be a Hybrid Energy Storage System (HESS) connected to the RTE's transmission grid during the project. On the contrary to the EPFL's demo, the Ringolab is under procurement and the figures included in this part are specifications and datasheets only. The HESS will be installed during the summer of 2020 and will run for a year before writing the final deliverables of the project.

#### 3.1.1 Size and layout of the Ringolab Hardware platforms

RingoLab will be a 1 MVA rated power fully containerized solution built by Ingeteam. The size of the solution had been chosen to fit into two 20-feets containers, having noted the available space in the destination substation. It includes a HESS consisting of six lithium-ion battery racks (0.5 MVA 60 min) and six supercapacitors racks (1MW-10s), and a 1 MVA Low Voltage (600V) inverter. Both, the energy storage system and the AC/DC converter have been sized and designed for a lifetime of 10 years. Moreover, the system can be installed outdoor as it has an IP54 certification.

All other required devices, including grid connection transformer, air conditioning, auxiliary and fire extinguishing equipment, are already installed in the container in order to limit on-site works and to perform FAT on the inverter before commissioning it in the substation. A layout of the container is shown in Fig. 3.1 and the single line diagram of the demo is shown in Fig. 3.2.

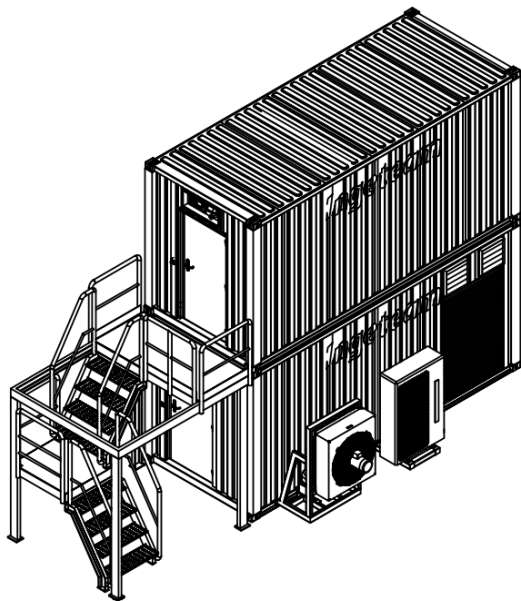


**Figure 3.1:** HESS layout

Main characteristics	
2 x 20' Container	IP54
AC/DC converter	1 MW
Transformer	20/0,6kV
supercapacitors	1MW-10s
Battery	0,5MW-60min

**Table 3.1:** Main characteristics

The inverter has voluntarily been undersized with respect to the total storage capacity. Indeed, the philosophy of the HESS is to deliver all fast acting services with the supercapacitor, while the battery will progressively replace it and ensure the steady-state/long-term service. Having an inverter in grid forming mode requires a very small amount of energy and only uses the power capacity for short time. The demonstration will assess the interest of such a configuration for this application and to what extent the sizing of the AC/DC converter is limiting the overall performance. In practice, a cost-benefit analysis will provide the optimal design of the installation. Here, we will investigate the main criteria that may drive this trade-off.



As seen on the Single Line diagram of the substation in Fig. 3.4, Castelet substation is composed of a 63 kV feeding busbar with:

- a 63 kV line to Ax Les Thermes substation,
- a 63 kV line to Tarascon-Ussat substation,
- a 10 MVA 63/20 kV transformer dedicated to a power hydro generation unit,
- a 20 MVA 63/20 kV transformer dedicated to the power supply of an industrial consumer with underground cable. The 1 MVA demonstrator will be connected to the secondary side of this transformer.

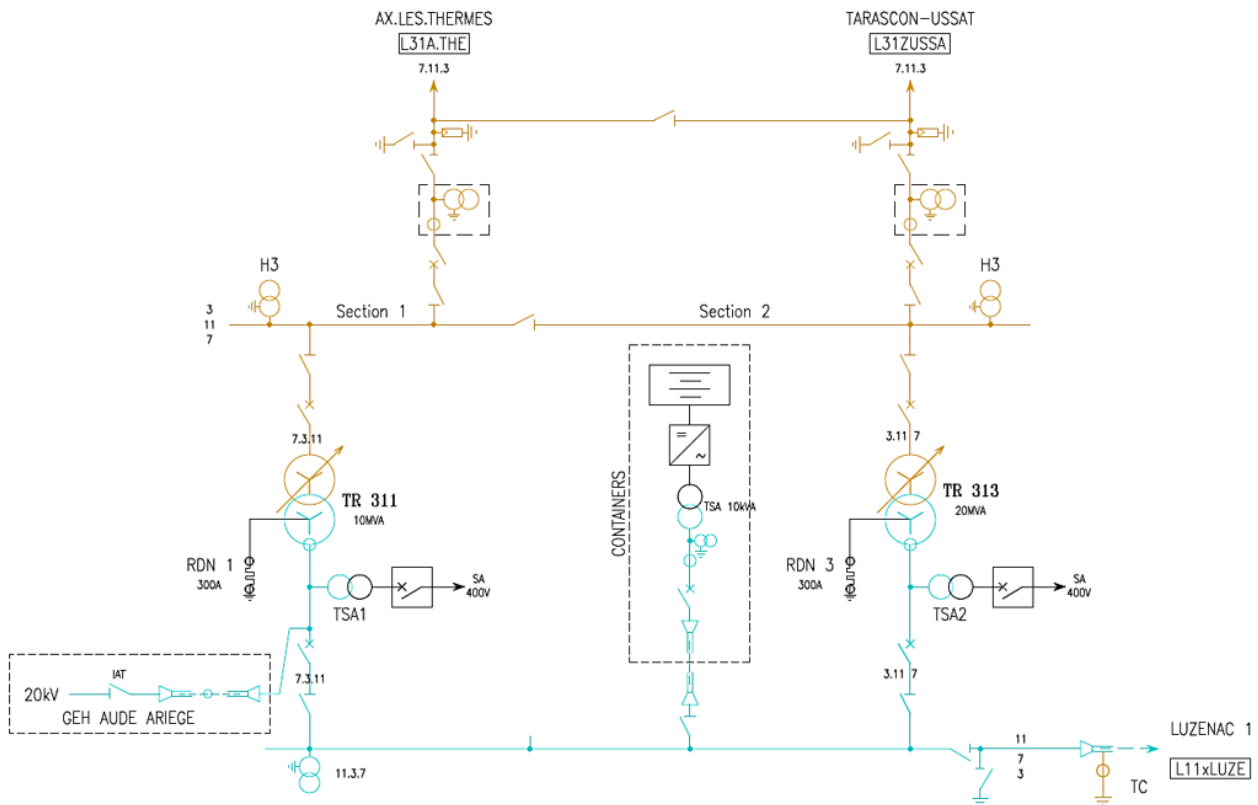


**Figure 3.4:** Destination substation - Single Line Diagram

According to the normal operation scheme, the small hydro powerplant is not supposed to be directly connected to the client and the HESS. Also, the HESS is not likely to be islanded with the client. Though, both situations can occur.

In general, the short-circuit power at the connection point is an indicator of the strength of the network, therefore the smaller it is, the higher the impact of the HESS on the grid. Neglecting the production connected at the 20 kV bus bar, it can be calculated as a function of minimal and maximum short-circuit current, which are provided in Table 3.2. The short circuit power at the 20 kV bus bar at Castelet ranges between  $58 \text{ MVA} < S_{sc} < 64 \text{ MVA}$ .

**Table 3.2:** Short-circuit currents simulated at the point of common coupling of the HESS

$I_{cc}$ 3-ph min (kA)	$I_{cc}$ 3-ph max (kA)	$I_{cc}$ 1-ph min (kA)	$I_{cc}$ 1-ph max (kA)
1.66	1.85	0.11	0.121

As aforementioned, the industrial load is expected to periodically start and make fast voltage angle and amplitude changes during the testing period. Figure 3.5 shows a sample of a Transient Fault Recorder (TFR) installed in February 2019 on the 20 kV bus bar where the HESS will be connected. We observe a load variation that presently occurs multiple times a day and that will stress the HESS.



**Figure 3.5:** Example of voltage and current measurement when switching on load

Regarding harmonic disturbances, the harmonic level at the substation of installation of the HESS is not negligible as shown in Fig. 3.6. Such harmonic level is compliant with RTE's rules from [24] which are recalled in Table 3.3, but is sufficient to challenge the HESS robustness compared to lab tests.

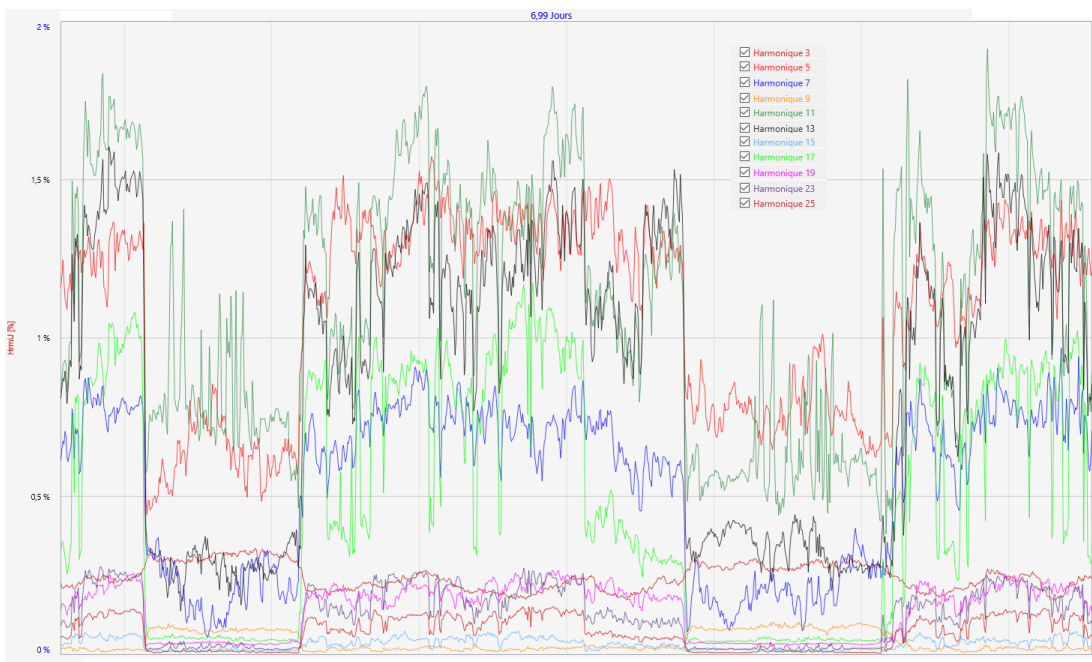


**Figure 3.6:** Example of voltage harmonics measurement for a week

**Table 3.3:** Harmonic requirements on transmission grid by RTE

Even Harmonics				Odd Harmonics	
non multiple of 3		multiple of 3			
order	max value	order	max value	order	max value
5 and 7	4%	3	4%	2	3%
11 and 13	3 %	9	2%	4	2%
17 and 19	2%	15 and 21	1%	6 to 24	1%
23 and 25	1,5%				

From the equipment point of view, Ingeteam design, as any HESS, must withstand the maximal admissible distortion of the voltage waveform considered in the connection grid with minor impact on it. In this project, the impact on and of the grid forming algorithm will be assessed.

Lastly, within one month of measurement data analysis, several single-phase fault were recorded in the connection point. One event is shown in Fig. 3.7.

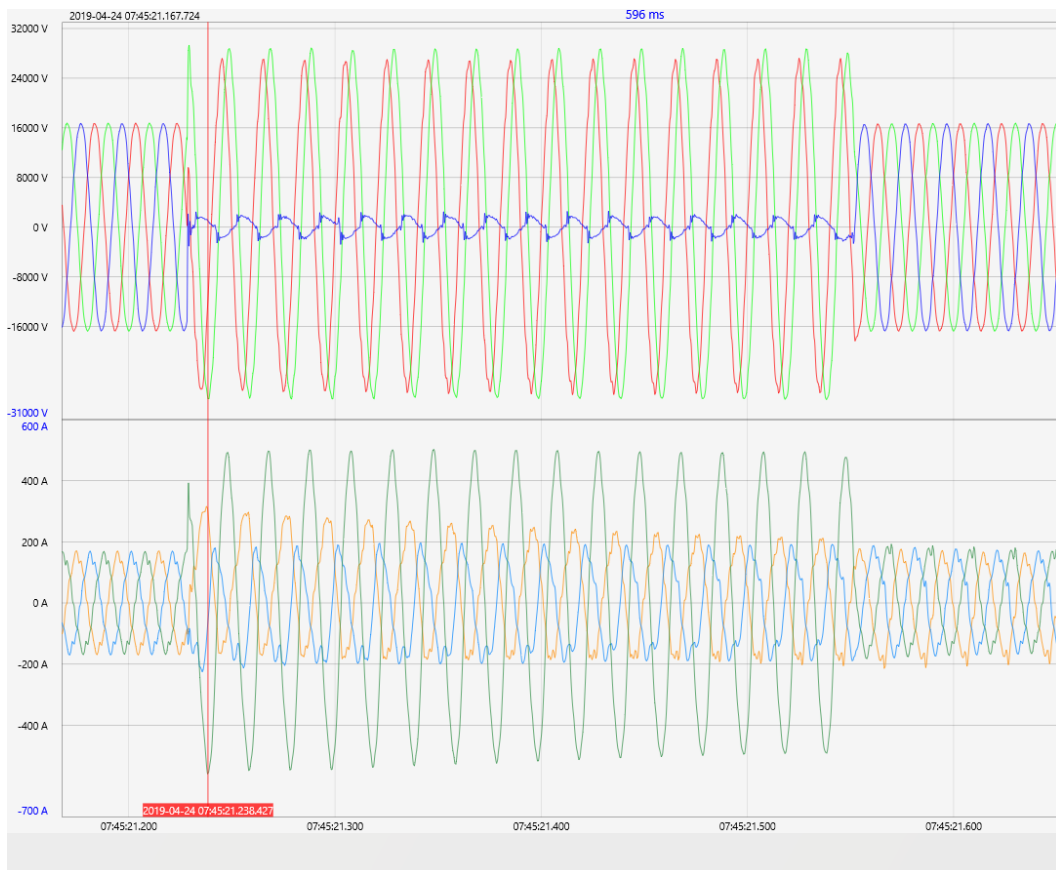


**Figure 3.7:** Single phase fault (20 kV, 24/04/2019). Up: Line-to-neutral voltages, Low: Line currents

### 3.1.3 Measures and data logging to support testing opportunities for Ringolab

The testing opportunities at the selected location for Ringolab due the disturbed conditions of the grid have just been highlighted. In order take advantage of these random events, monitoring capabilities and a suitable communication infrastructure are proposed as depicted in Fig. 3.8.

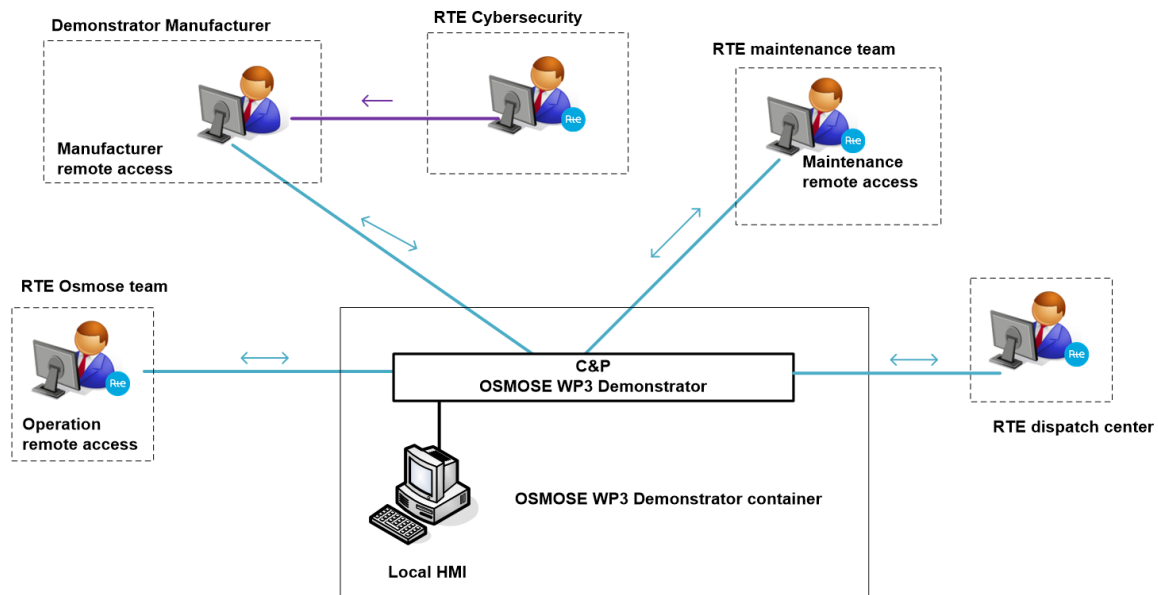


**Figure 3.8:** Telecommunication infrastructure

The chosen organization will allow remote access to on-site measurements, to send reference set-points by the OSMOSE team under the supervision of the control center, and to send alarms to different actors for maintenance purposes. All the control parameters and setpoints to be sent to the HESS will also be stored. Not being exhaustive, this list includes:

- active and reactive power references of the AC/DC inverter,
- voltage and frequency references of the AC/DC inverter,
- the activated services,
- references for DC/DC converters when they differ from the AC/DC references.

The electrical measurements will be provided by the internal measurement system of the HESS, but also by the aforementioned dedicated TFR [25]. Indeed, since the grid forming control is sensitive to grid changes, it is of crucial importance to analyze grid measurement prior to the installation of the HESS. Currently, two types of signals are continuously recorded:

- Average 10 min values of:
  - voltage frequency per phase,
  - voltage amplitude per phase,
  - voltage harmonic values from 1 to 50,
  - voltage unbalance, with positive, negative and zero sequence,
  - current amplitude,
  - current harmonics from 1 to 13,
  - current unbalance with positive, negative and zero sequence.
- waveform recording of all voltages and current for 10 sec with a sampling rate of 10,24kHz triggered on:
  - voltage amplitude variation (threshold at 3%)
  - phase shift (threshold at 3%)

The triggers may be adjusted following the analysis of the a few measurement campaign.

---

The HESS SCADA will manage all the alarms and data logging of the system, which will be stored in the local PC. This includes:

- Display alarms of Power Converter System (PCS) and Battery Management System (BMS).
- Email reporting of alarms and daily operation in excel tables.
- Report to the Customer SCADA/Control Centre of the required information for generation of the monthly performance reports for RTE.
- The commands entered through the HMI, with at least the date, user and input command.

In addition, the SCADA can take samples from several hundreds of milliseconds to few seconds and stores the data in an internal buffer (several hours or days). Once the buffer is full, the data is downloaded to the local PC. The data stored in the PC depends on the hard drive capacity and can go from months to years. The SCADA can store values of the following variables among others:

- active and reactive power injected by the inverter,
- current injected by the inverter (module),
- Voltage at the terminals of the inverter (module),
- DC bus voltage,
- batteries voltage, output current and SoC,
- capacitor voltage, output current and SoC,
- output current, SoC and temperature of each Rack.

Having raw measurements of electrical data from the site will allow us to post process them using the same PMU algorithms as in the EPFL demonstration [8], ensuring fair comparison amongst measurement locations and demonstrations.

## 3.2 Implementing grid forming control in Ingeteam inverter

The MIGRATE project developed different grid forming controls and current limitation strategies. These models have been made available on-line following an open source policy [26]. The control structure is based on classical cascaded loops with a current control loop, a voltage control loop and an outer control loop for controlling the active power and reactive power under a droop scheme strategy, while the power part is represented by averaged voltage sources.

The control algorithm is modelled considering continuous time and the grid connection transformer as an inductance. This first scenario was analyzed and some setting were changed in order to make the control model compatible with a grid-connected real hardware implementation. Moreover, some MIGRATE simulation parameters were updated to take into account the physical characteristics of the Ringolab equipment as will be installed on RTE's grid, such as the filter and transformer impedance. DC/DC converter were modeled as ideal voltage sources with a RL connection impedance.

### 3.2.1 Required control algorithm updates

Then, the following components were added as they are the key for smooth and reliable operation of the HESS in any condition and an accurate representation of fast transients:

- converter protection subsystems,
- saturation and limits for external set points,
- introduction of a state machine (see Fig. 3.10),
- synchronization (and a PLL).

Main modifications are summarized as a flow chart in Fig. 3.9. The time steps presented in the chart are the one used in the hardware.

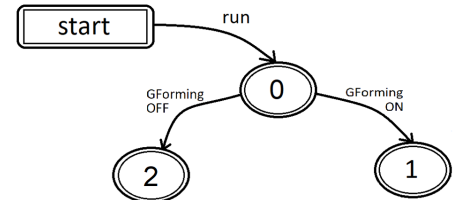
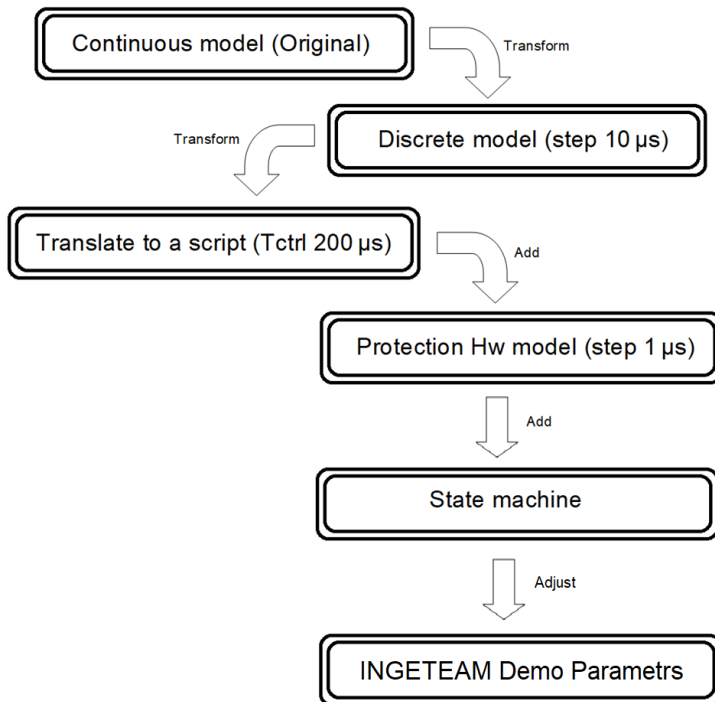


**Figure 3.10:** State machine implemented in Matlab-Simulink

**Figure 3.9:** Model adaptation flow chart

The converter output current is thermally limited as it is impossible for the semiconductors to conduct a 2 p.u. current if they were not specifically designed for it. Usually, when the current increases without control, (during fast uncontrolled transients, below some hundreds of microseconds), the converter has protection subsystems to curtail the output current and prevent fatal damage. Those subsystems, do not act during normal operation, but they can significantly affect transients during some hard disturbances such as phase shift, short circuits, or voltage dips amongst others. As the scope of the analyses includes the accurate transient responses, they must be taken into account.

In a similar way but in the steady state framework, control loops should not set a reference that the real hardware cannot handle. Therefore it is important to implement some saturation procedures according to the converter hardware limits to prevent the control loop from generating a voltage level impossible to synthesize by the hardware. The unsolvable gap between the reference and the generated voltage may lead to instability. The control strategy proposed in the MIGRATE project is a grid forming control with external active and reactive power setpoint. Thus, for those external setpoints, same limitations as for a grid following control are proposed in the new approach.

Finally, the management of the model under different operation modes or even faulty modes imposes the definition of a state machine. The state machine enables / disables different control structures or code parts depending on pre-programmed logics. Therefore, it is possible to use an algorithm to synchronize the converter to the grid the first time and then another one for normal operation. Depending on the grid / converter conditions and the user commands, the AC/DC converter will execute a control code or another.

Moreover, in order to smoothly synchronize the converter on the connection to the grid, the implementation of a PLL is mandatory. Although, this PLL based structure is not used during normal operation. More details about these components are given below.

---

### 3.2.1.1 Converter Protection Subsystem

The current saturation scheme developed within MIGRATE project is implemented in the RingoLab control. But a simple logic to open (shutdown) semiconductors has been added in order to curtail the output voltage/current and prevent fatal damage of the converter in case the limitation strategy fails to keep the current/voltage within admissible range during the very fast first uncontrolled transient. When voltage or current values are potentially destructive for the converter, semiconductors are opened (and blocked). This hardware based protection layer avoids damage for the equipment, but it may lead to a disconnection. Thus, this protection logic is the last one to be activated.

### 3.2.1.2 Saturation and limits for external setpoints

A power converter has two main limitations in continuous operation:

- Current, thermally limited
- Maximum output voltage. Depends on DC Bus voltage and system parameters.

The maximum output voltage is closely related to the converters capability to inject capacitive reactive power. In the proposed solution, the maximum reactive power is estimated based on the DC bus voltage and the voltage at the point of common coupling (PCC). Thus, if any of the power set points is bigger than the maximum, one or both set points (P and/or Q) should be modified. Assuming grid forming control will never try to increase grid voltage from the external set point value (and a low injected active power), PQ limits based on the voltage set point can be estimated. As first approach, same limitations as grid following control with active power priority control have been implemented.

### 3.2.1.3 Supervision State Machine

As aforementioned, the state machine is used to manage the control algorithms. The first version of the state machine has 3 different states as illustrated in Fig. 3.10:

- 0: Synchronization, used when the HESS starts and needs to smoothly connect to the grid,
- 1: Grid Forming, normal mode of operation,
- 2: Grid Following, fallback solution / testing procedure. This mode might be used in case of emergency or malfunction of a part of the storage that allows grid forming.

### 3.2.1.4 Synchronization pre-connection

A PLL based algorithm is implemented in order to synchronize the AC/DC converter with the grid. The output voltage of the converter is increased with a low derivative (low enough not to excite the grid connection filter resonance). Once the output voltage of the AC/DC converter and the grid are synchronized, the main breaker is closed. Figure. 3.11 illustrates this procedure.

## 3.2.2 Performance validation through simulation of MIGRATE test-cases

Validation of the updated control is performed on the same test cases proposed in MIGRATE, but rescaled in power, as they cover several prototypical scenarios based on a single converter connected to an infinite bus.

- Case 1-A-1: Islanding of a power converter.
- Case 1-B-2: Tracking power and voltage references when connected to a strong grid.
- Case 2-A-1: Response to grid events (i.e., disconnection of a line and short circuit faults).

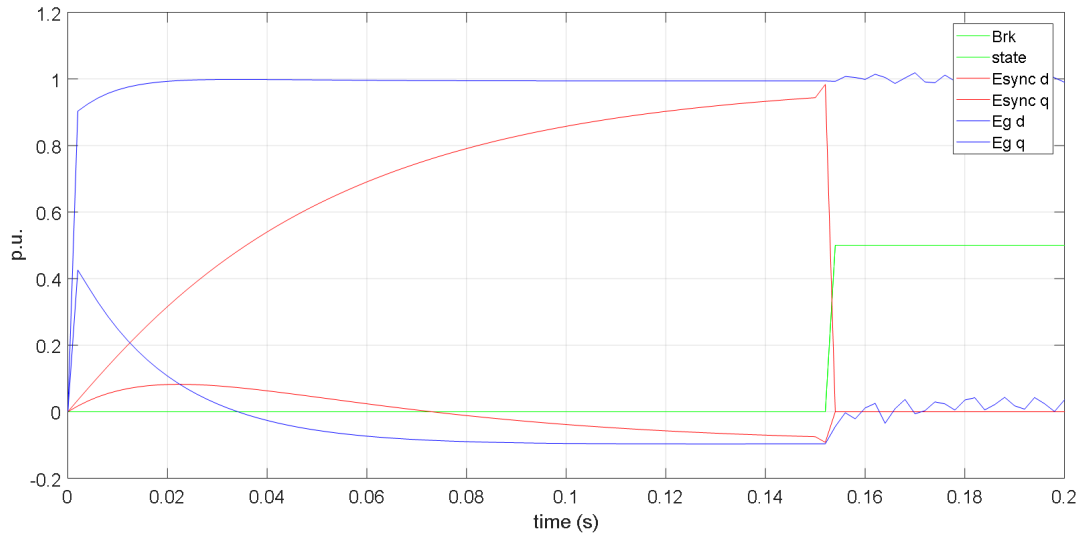


**Figure 3.11:** Synchronization process results obtained in Matlab-Simulink

### 3.2.2.1 Test case 1-A-1: Islanding

A single converter connected to an infinite bus as shown in Fig. 3.12 is used to study the behaviour of the different system-level controls during islanding.

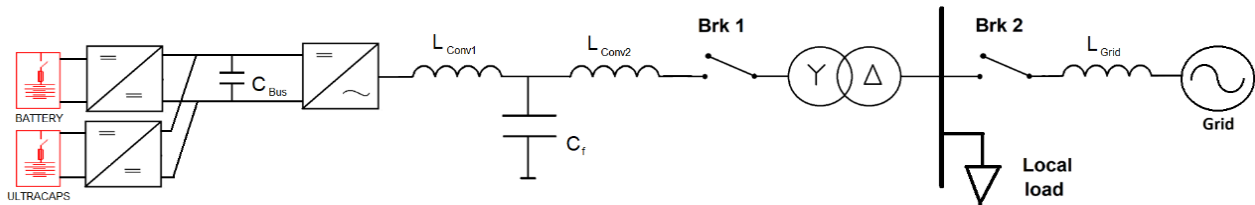


**Figure 3.12:** Single bus case study used to check the ability of the converter to operate in islanded mode (disconnected from the grid, Brk 2 = 0).

In this scenario, the switch Brk2 opens at  $t = 0.5s$  and islands the converter and the local load. A constant power load of  $-100\text{ kW}$  is enabled at  $t = 2s$ , then, the load changes to  $100\text{ kW}$  at  $t = 3.5s$ . Simulation results for this scenario obtained with the average MIGRATE model (thin curve) are superimposed with the results of the new electromagnetic model (thick curve) in Figs. 3.13 and 3.14.

### 3.2.2.2 Test case 1-B-2: Reference tracking when connected to a strong grid

A single converter connected to an infinite bus as depicted in Figure 3.15 is considered. This test case is used to check the ability of the different system-level controls to track references for the active power injection and the terminal voltage when connected to a strong grid. In this case, the switch Brk2 is closed and the impedance of the infinite bus is computed based on a short circuit ratio of 20. In this simulation both references, active power injection and voltage at converter terminals are varied to check the ability of the power converter to track the references. The voltage reference is set to  $E_{set} = 0.95\text{ pu}$  at  $t = 0.5s$ ,  $E_{set} = 1.05\text{ pu}$  at  $t = 1s$ , and  $E_{set} = 1.0\text{ pu}$  at  $t = 1.5s$ . Moreover, the active power reference is changed to  $P_{set} = 800\text{ kW}$  at  $t = 2s$ ,  $P_{set} = -800\text{ kW}$  at  $t = 3s$ , and  $P_{set} = 0$  at  $t = 4s$ . Results for this scenario are shown in Figs. 3.16 and 3.17.

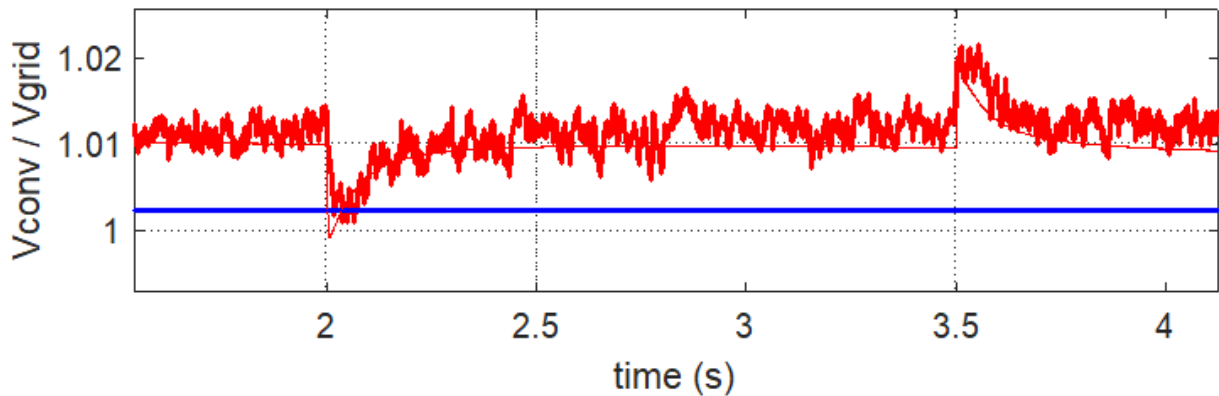


**Figure 3.13:** Simulation results for case 1-A-1, converter and grid voltage. Results of the average MIGRATE model (thin curve) superimposed with the results of the new model (thick curve).

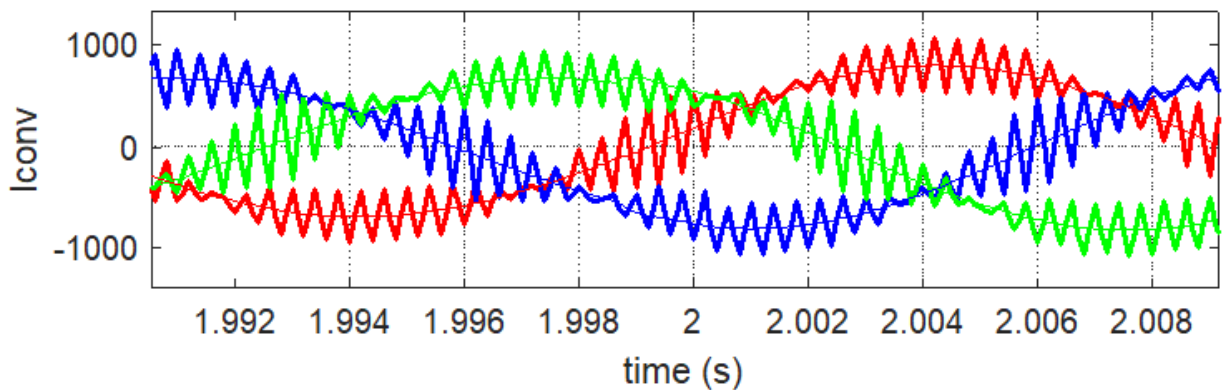


**Figure 3.14:** Simulation results for case 1-A-1, converter RST currents. Results of the average MIGRATE model (thin curve) superimposed with the results of the new model (thick curve).

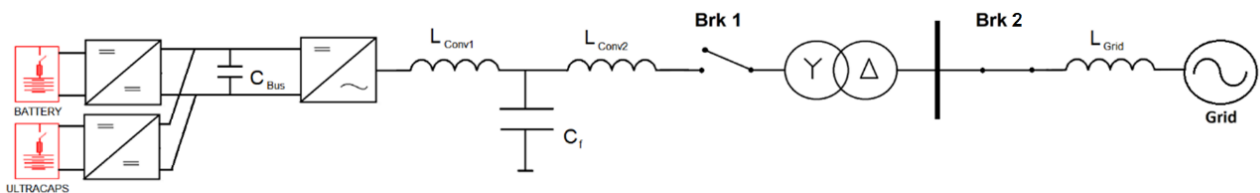


**Figure 3.15:** Single bus case study used to check the ability to track references for the active power injection and the terminal voltage.

In this section also, the results obtained with the average MIGRATE model (thin curve) are superimposed with the results of the new electromagnetic model (thick curve). The control algorithm regulates the output voltage of the converter in order to meet the set point within 200ms from the change in the voltage reference. Active power external reference is sloped. But, in roughly 300ms, the system can vary its output active power from zero to 80% of the rated power.

The biggest difference compared to the MIGRATE project results can be found in the injected current when voltage reference is changed ( $t=0.5s$  to  $1.5s$ ). The difference is caused by an impedance mismatch. The MIGRATE model with respect to the new approach has different grid connection filter impedance. Hence, this effect is not caused by the control algorithm.

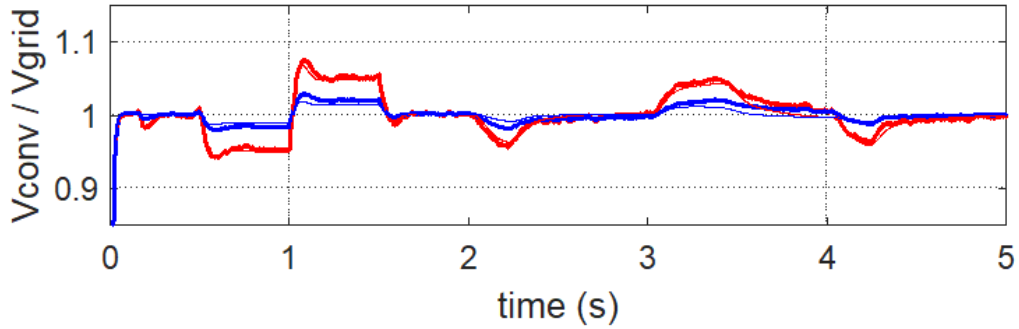


**Figure 3.16:** Simulation results for case 1-B-2, converter and grid voltage. Results of the average MIGRATE model (thin curve) superimposed with the results of the new model (thick curve).

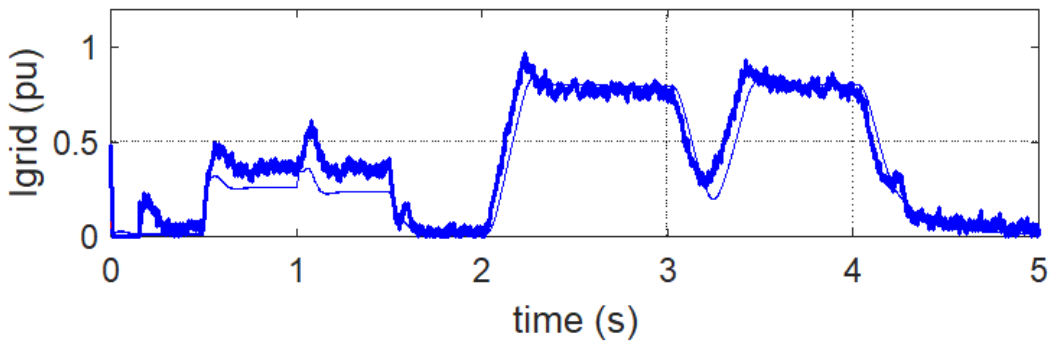


**Figure 3.17:** Simulation results for case 1-B-2, grid current module. Results of the average MIGRATE model (thin curve) superimposed with the results of the new model (thick curve).

### 3.2.2.3 Test Case 2-A-1: Short circuit fault and line opening

In this part, the response of a single power converter to a short circuit fault using the case study depicted in Fig. 3.18 is investigated. A three-phase short circuit fault occurs on the line 2 at  $t = 1.5\text{s}$  and is cleared by disconnecting the line (BrkL1\_A and BrkL1\_B) after 150ms. The purpose of this case study is used to verify the compatibility between system-level controls and the current limitation scheme of the device level control. Simulation results are shown in Figs. 3.19 and 3.20.

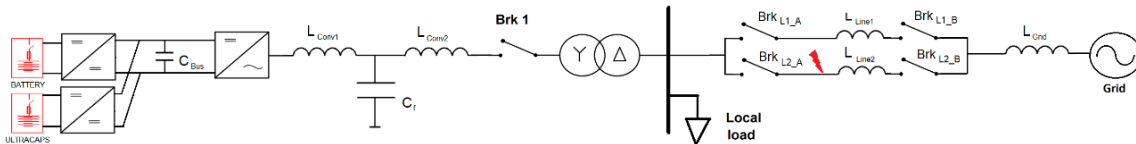


**Figure 3.18:** Single bus case study used to check the stability and the ability to withstand large transients after a short circuit fault.

In this case, the results obtained with the average MIGRATE model (thin curve) are slightly different from the results of the new electromagnetic model (thick curve), which is explained by the activation of the IGBT blocking protection subsystem at the beginning and at the clearing of the fault. Despite the difference in the transients, same steady state values are achieved in both cases and the control algorithm rides through the fault. The converter it is not disconnected from the grid during the event.

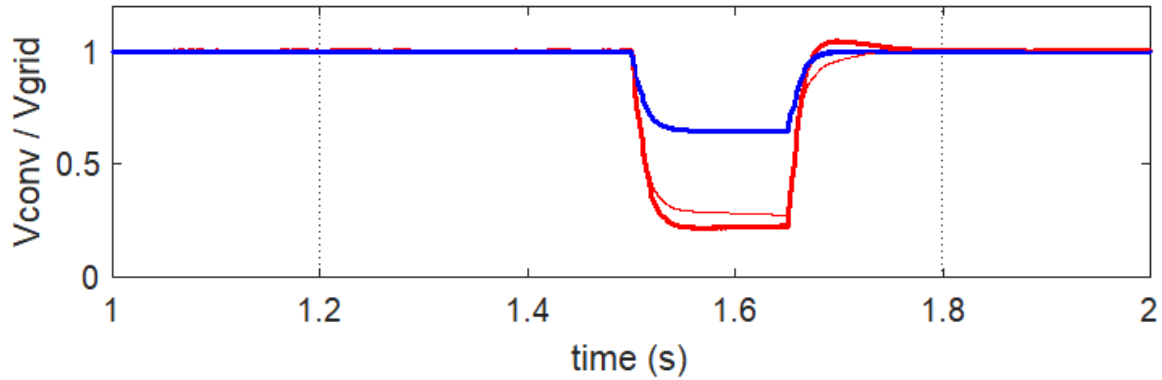


**Figure 3.19:** Simulation results for case 2-A-1, converter and grid voltage. Results of the average MIGRATE model (thin curve) superimposed with the results of the new model (thick curve).

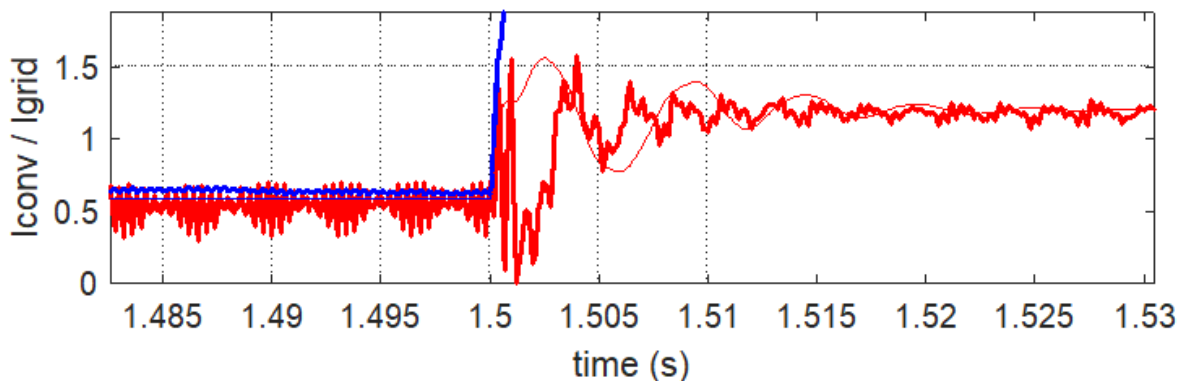


**Figure 3.20:** Simulation results for case 2-A-1, converter and grid current modules. Results of the average MIGRATE model (thin curve) superimposed with the results of the new model (thick curve).

### 3.2.3 Discussion on MIGRATE control limits for RingoLab application

#### 3.2.3.1 Behaviour under unbalanced faults

Grid unbalanced voltage faults were not addressed in MIGRATE project. The control structure used in MIGRATE project is capable to ride through some faults and a certain degree of unbalanced voltage. Nevertheless, not all the requirements in the standard grid codes are fulfilled.

Fault current at converter terminals during a deep unbalanced fault has a strong negative component (see Fig. 3.21). Considering the virtual impedance protection subsystem, each negative sequence period, the virtual impedance could be activated and de-activated behaving as a non-linear load. Resulting converter current would have an undesirable high low order harmonic components (see Fig. 3.22). To ensure correct behaviour of the converter at all grid conditions control improvements should be proposed and implemented later on.

A straightforward solution would be to control the negative sequence of the AC/DC converter voltage, through current and power control and feedforward terms as proposed in [27], [28], [29]. However, the usual objectives in the literature is to remove active power oscillations and current ripples, while we want to prioritize the voltage. Indeed, unbalanced loading necessary implies power oscillations. In addition, sequence separation induces computation delays that endanger the current limitation effectiveness in practice. Alternatively, independant phase limitation in time domain could be a solution.

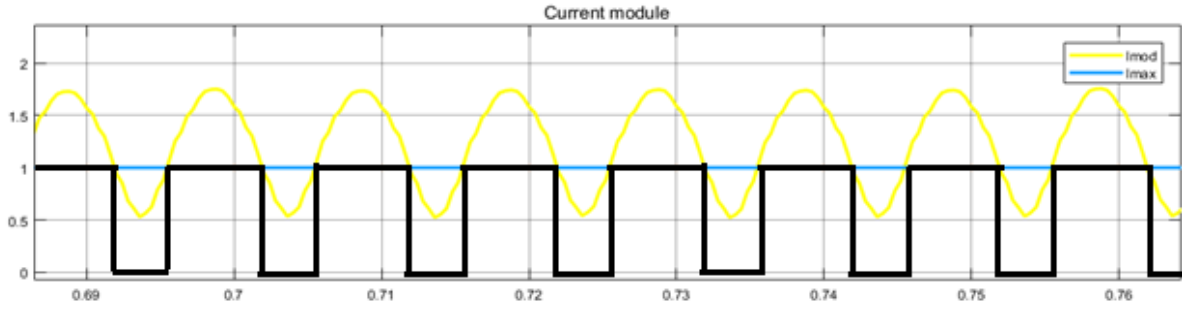


**Figure 3.21:** Current module at severe voltage unbalances

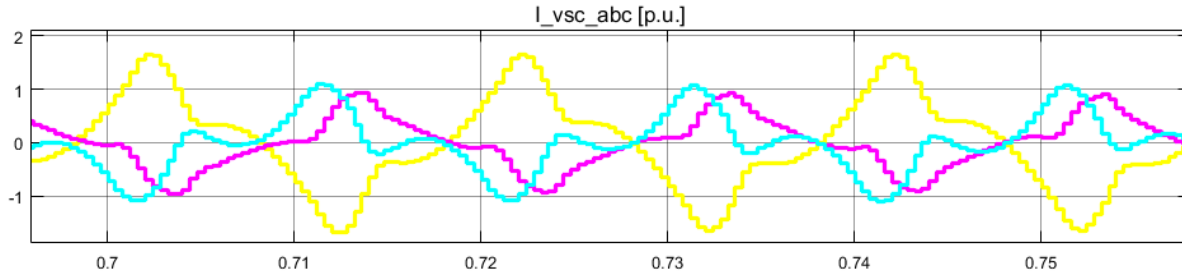


**Figure 3.22:** Converter output current while virtual resistor is operating as a non-sinusoidal load.

### 3.2.3.2 Finite DC side energy

The controls developed within MIGRATE WP3 [26] are all making the AC/DC converters providing primary frequency control. Indeed, in steady-state, the power delivered by a grid-forming converter with filtered droop control is [2]:

$$P = \frac{\omega - \omega_{ref}}{k_d} + P_{set}$$

Since services at RingoLab are expected to be decoupled from each other and a limited storage capability is available, the controls must be adapted to provide grid forming alone without permanent PFC. A first proposal made in [3] consists in stopping the system from providing PFC when the state of charge (SoC) of the battery is going too low or too high. Again, this control cannot be applied at the RingoLab as the battery might be testing without PFC even with the adequate SoC.

For this project, a **transient grid forming control mode** is proposed which ensures that the AC/DC inverter will deliver a power equal to its setpoint by making the frequency reference equal to the network frequency filtered with a 1st order low pass filter. Thus the inverter will behave as a grid forming inverter during transients but its power will come back to its reference even in case of frequency deviation. The dynamics of this strategy will depend on the time constant of the first order low pass filter and will be studied in subsequent stages of the project.

$$P - P_{set} = \frac{1}{k_d} \omega - \frac{\omega_{network}}{1 + T_{LPS}}$$

## 3.3 DC side converter control developments

In the framework of this project, battery / supercapacitor (SC) passive hybridization is discarded. For passive hybridization very accurate knowledge and models for battery and SC are needed. Furthermore, depending on the SoC, the batteries will have a different voltage and impedance.

DC bus bar of the converter and its harmonics have to be also taken into account. For these reasons, active hybridization by controlling DC/DC converters is proposed in the RingoLab demo.

It is recalled the RingoLab includes:

- for the battery: 1 hour and 500kW. It will therefore be possible to test different services and maintain it for the following hour ideally.
- for the supercapacitor: 10 sec and 1MW to feed the grid transients before traditional primary frequency control reacts.

Then, different strategies could be used for controlling the DC/DC converters, which might entail coordination with the AC/DC inverter or be only dependent on the DC bus voltage. Research on this topic has been mainly conducted in the context of electric vehicles (EV) [30,31].

Indeed, EV applications require both high power (acceleration and deceleration/regenerative braking phase) and high energy (range). The grid forming application, with fast power transient is closer to the EV application than previous application on the transmission grid.

In this section, different control strategy suitable to fulfill DC side energy management requirements and performances will be discussed. Here, we propose to separate DC/DC controls in 2 hierarchical layers that will be further detailed in the following:

- the "power" control dealing with power sharing between the supercapacitor and the battery and,
- the "energy" control managing the energy in both supercapacitor and battery.

### 3.3.1 Power sharing controls strategies for DC/DC converters

Control strategies based on power sharing in hybrid systems often require an extra-control loop to regulate the supercapacitor state of charge, which may be difficult to implement. For this reason, some control strategies are based on master/slave schemes in which only one source (supercapacitor based) controls the DC bus voltage and the other (battery based) only controls the power.

For instance, the power set point of the battery could be fixed to a user defined value or given by the AC/DC converter, whereas the supercapacitor regulates the DC bus voltage as shown in Fig. 3.23.

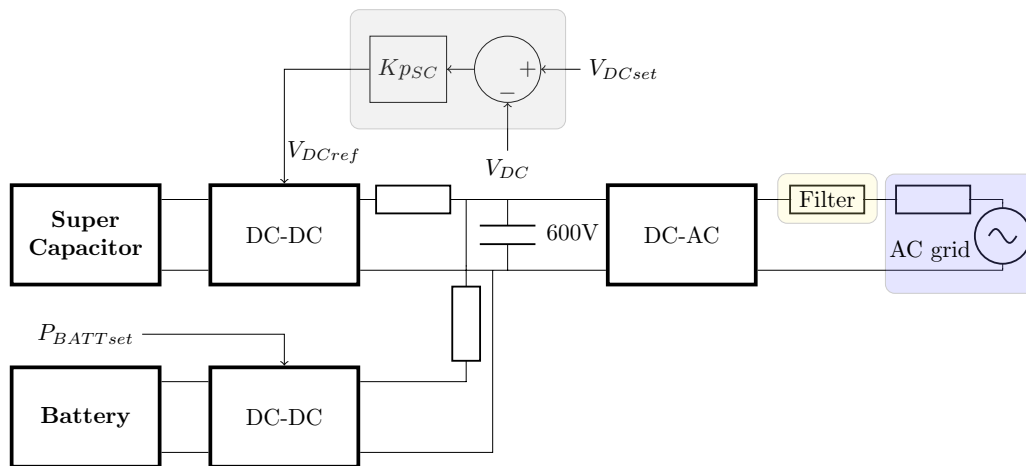


**Figure 3.23:** Bloc diagram of Fixed battery + Supercapacitor regulating voltage

Besides simplicity, the main advantage of this approach is that the dynamics of the battery is easily controlled. Its main drawback is that DC bus voltage is only regulated by one device, which means that in case of failure of the supercapacitor, this important function is not longer ensured. Then, a specific procedure is required to handle supercapacitor malfunctioning. Therefore, this option is likely to be disregarded for our grid forming HESS application in favor of approaches like the followings.

### 3.3.1.1 Control 2: Virtual RC control

The virtual RC control applied to the HESS consists in 2 independent control loops, as shown in Fig. 3.24, that are decoupled designed and enable the parallel operation of both DC/DC converters.

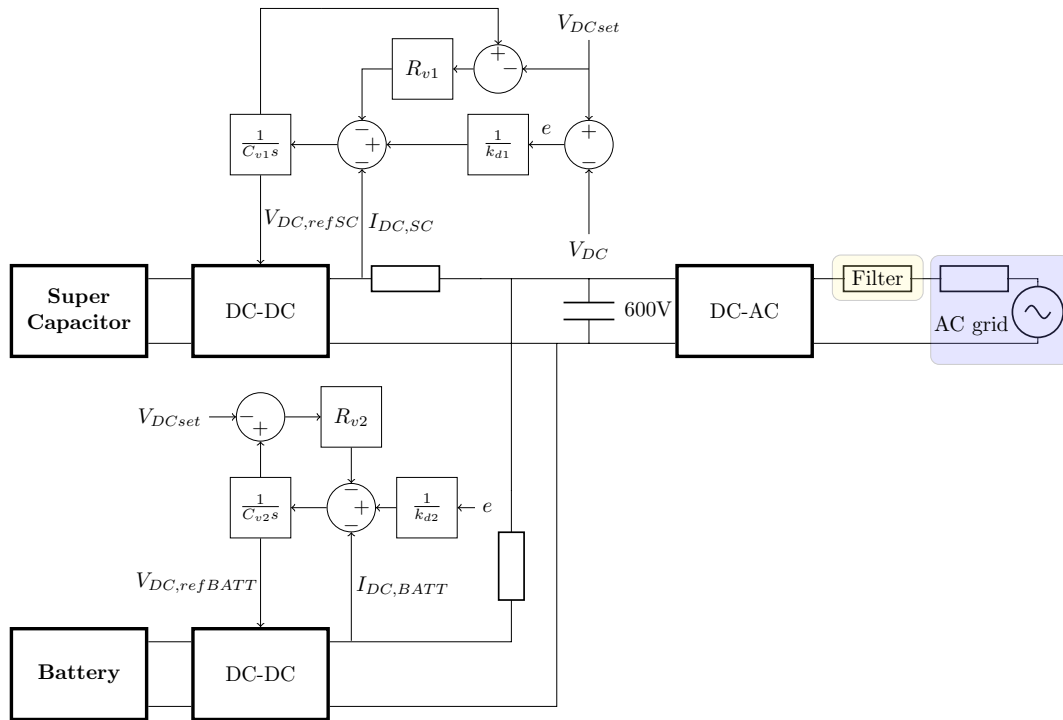


**Figure 3.24:** Virtual RC scheme for transient sharing of the DC power

Following this strategy, both storage systems, the battery and supercapacitor, are responsible for the DC bus voltage regulation through a steady state droop. Then, the dynamic of each DC device is driven by its own virtual RC circuit, which can be set independently. DC/DC converter related to the supercapacitor must have a fast transient current response and a low stationary droop gain, while the battery system should react slowly to transients but exhibit a high stationary droop gain. The relation between the control parameters and DC side performances can be summarized as follows:

- In steady state: depending on the voltage difference ( $V_{DCset} - V_{DC}$ ), a droop control is established. Droop curve parameters are ( $K_{d1}/K_{d2}$ ).
- Transient current depends on the time constant of the equivalent “virtual RC circuit” given by:

$$\frac{C_{v1} * R_{v1}}{C_{v2} * R_{v2}}$$

Figures 3.25-3.28 show simulation results for different values of the control parameters to illustrate the sensitivity of the performance to the tuning.

However, this control strategy requires additional outer loops.

- at least one for assuring that the steady state power output of the supercapacitor is equal to zero. This can be achieved by using as a DC voltage reference for the supercapacitor a filtered value of the DC voltage. The time of the filter will define how fast the current goes to zero after the transient.
- another to ensure that the supercapacitor energy is equal to half of its maximal capacity. This can be done using an integral controller on the SoC that will modify the DC voltage reference.

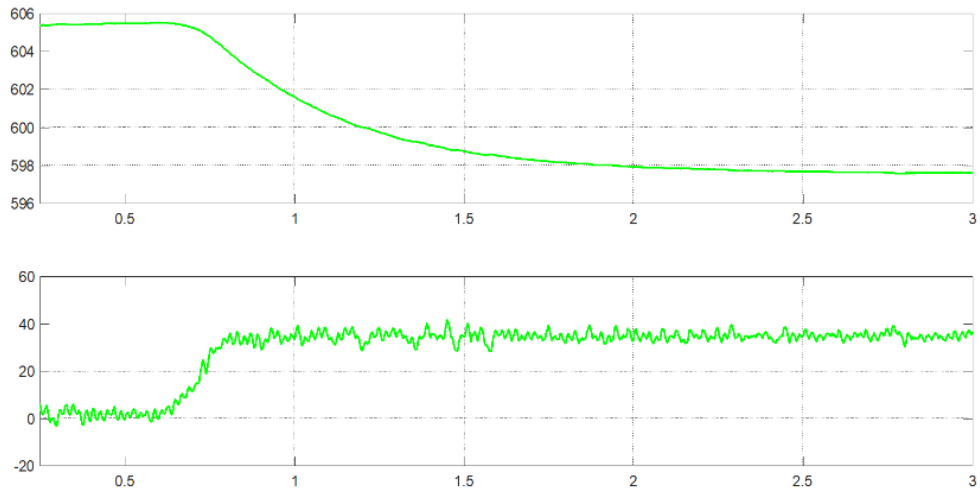


**Figure 3.25:** DC/DC converters response for an active power step same values for both DC/DC (arbitrary choice)

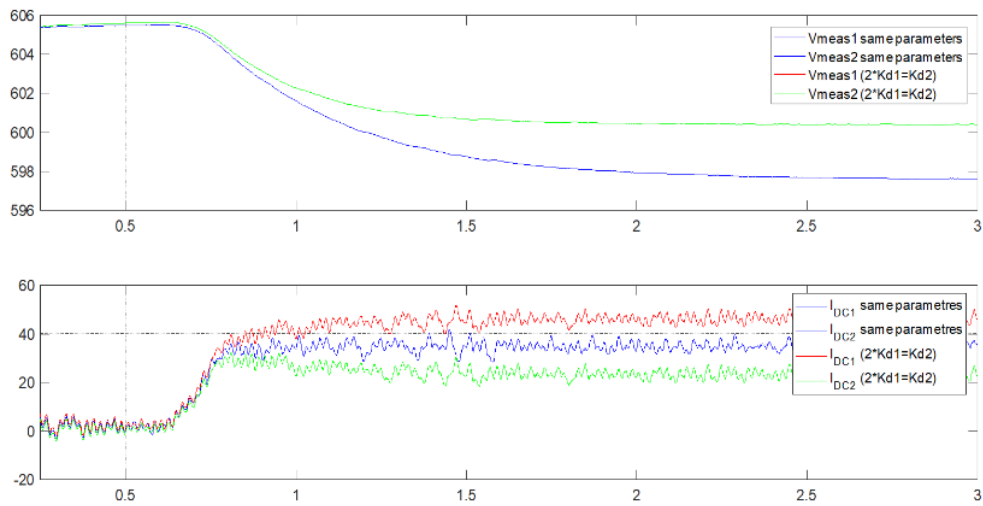


**Figure 3.26:** DC/DC converters response for an active power step  $Cv1=Cv2$  and  $Kd1=Kd2/2$

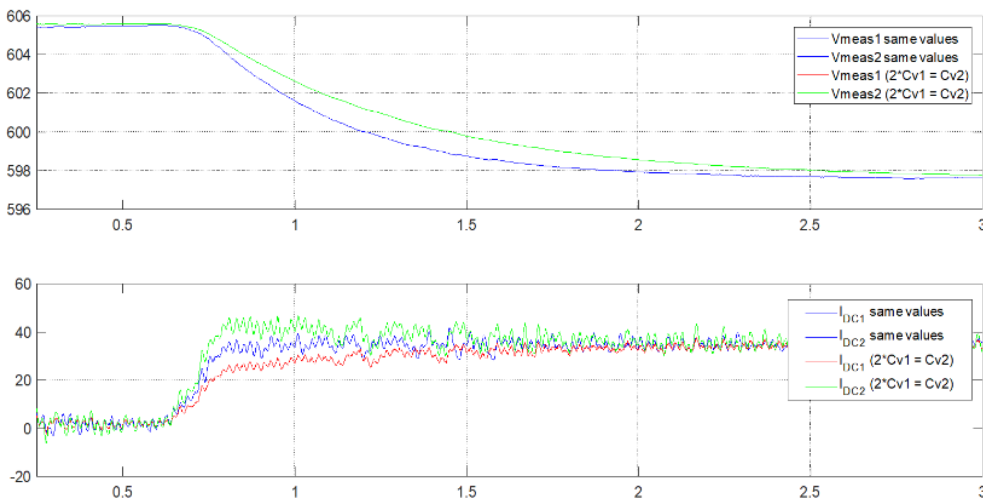


**Figure 3.27:** DC/DC converters response for an active power step  $Cv1=Cv2/2$  and  $Kd1=Kd2$

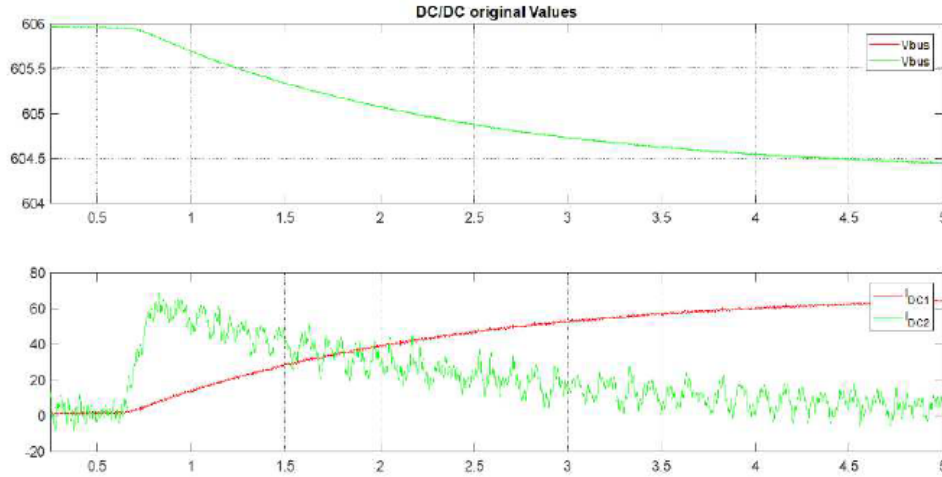


**Figure 3.28:** response of the scheme to active power step

### 3.3.1.2 Control 2: PIP control

Above requirements can be met using a proportional-integral (PI) controller on the battery and a P controller on the supercapacitor as shown in Fig. 3.29. Having only a P controller on the supercapacitor allows its contribution to be null in steady state, while the I controller on the battery ensures that the DC voltage reaches its setpoint in steady state. This strategy could be applied to the current instead of the power. The ratio between the proportional gain of the battery and the supercapacitor regulates their relative dynamics following a change in the DC voltage.

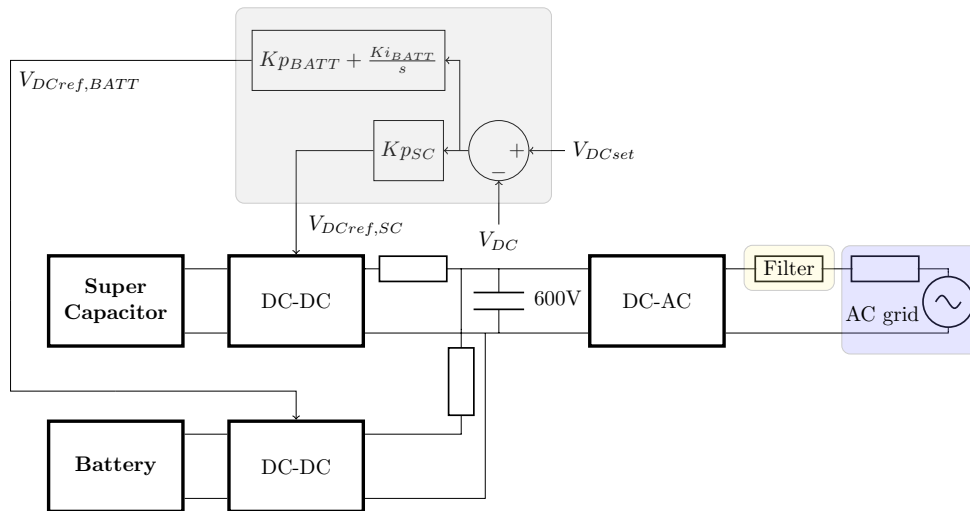


**Figure 3.29:** Bloc diagram of the PIP controller

Neglecting the dynamics of the RL impedance that connects the DC/DC converters, the dynamics of the current of the supercapacitor and the battery are given by:

$$I_{SC} = I_{invAC} \frac{Kp_{SC}s}{Cs^2 + (Kp_{Batt} + Kp_{SC})s + Ki_{Batt}}$$

$$I_{Batt} = I_{invAC} \frac{(Kp_{Batt}s + Ki_{Batt})}{Cs^2 + (Kp_{Batt} + Kp_{SC})s + Ki_{Batt}}$$

where  $I_{invAC}$  is the current flowing from the DC capacitance to the AC/DC inverter. Since the capacitance of the DC bus will be extremely low, we can neglect it and write:

$$I_{SC} = I_{invAC} \frac{Kp_{SC}s}{(Kp_{Batt} + Kp_{SC})s + Ki_{Batt}}$$

$$I_{Batt} = I_{invAC} \frac{Kp_{SC}s + Ki_{Batt}}{(Kp_{Batt} + Kp_{SC})s + Ki_{Batt}}$$

This shows that the dynamic behavior of the DC side will be driven by the ratio  $Kp_{SC}/Kp_{Batt}$ . As this ratio increases, the same occurs with the contribution of the supercapacitor to disturbances. In steady state  $I_{Batt} = I_{invAC}$ . Figures 3.30 show the power output of the DC/AC inverter, battery and supercapacitor for 2 types of event on the grid, considering a ratio  $\frac{Kp_{SC}}{Kp_{Batt}}$  equal to 100:

- Angle shift of 0.1 rad (5.7deg) and,
- frequency variation of 1%.

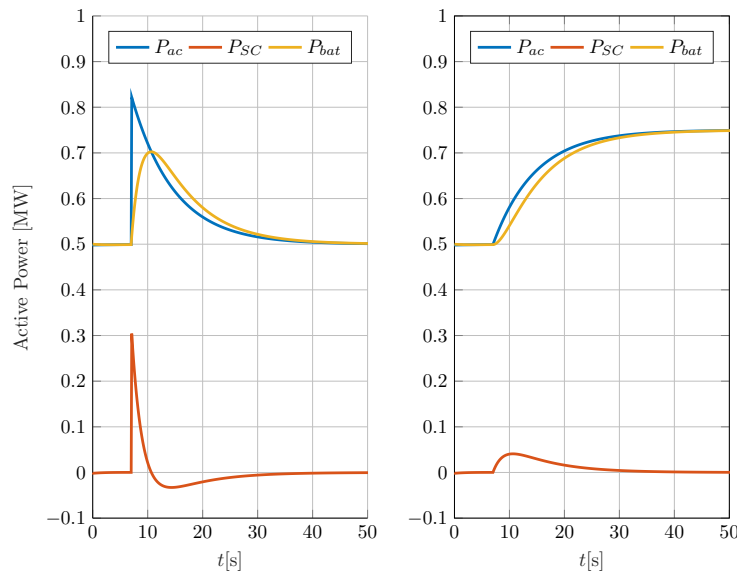


**Figure 3.30:** Active power of AC/DC converter, supercapacitor and Battery following: a angle step change of 0.1 rad (left), frequency step change of 0.01 p.u (right)

It is observed that, as expected, the supercapacitor react very fast while the battery is subject to a low  $\frac{dP}{dt}$ . This control strategy has the advantage of setting both the battery and supercapacitor in charge of the regulation of the voltage at the DC bus. Therefore in case of failure of one of them, the DC voltage will remain controlled and the inverter could be maintain in operation (even if some emergency scheme might smoothly shut it down).

At this stage of the project, the most interesting possibilities related to the control & management of the supercapacitor & batteries hybrid system have been considered. The final choice will be made in a later stage, based on practical analyses and implementation constraints, by taking into account all possible events that might happen and how to handle them in a safe way.

### 3.3.2 Energy management controls for the HESS

This experimentation has a reduced amount of storage, therefore maintaining an adequate SoC is vital to ensure proper operation of the devices. As the time constant of the energy buffer in the supercapacitor and the battery have two orders of magnitude difference, we will deal with them separately.

### 3.3.2.1 Energy in the supercapacitor

As aforementioned, the supercapacitor will mainly deal with providing the fast transient response required by of the grid former control implemented in the inverter. These transients can lead to both an increase or an decrease of the power with respect to the predefined value. Therefore, the control must be able of charging or discharging the supercapacitor at any moment. It means that the supercapacitor SoC should be at a half of its full charge. Here, we propose an outer loop to slowly bring the energy of the supercapacitor back to this value. The energy may come from 2 sources:

- the battery, with an amount of energy that can be assumed to be almost infinite compared to the supercapacitor,
- the network.

Having one source balancing the supercapacitor will induce slow and small deviation of its power output while the other source will show a more still output. The amount of energy to keep the supercapacitor charged will be in average very small compared to the amount of energy in the battery or the network. Since the supercapacitor has the very interesting property of expressing its SoC as a direct function of it voltage:

$$E_{SC} = \frac{V_{SC}^2}{2},$$

having  $E_{SC} = \frac{E_{SCmax}}{2}$  is equal to have  $V_{SC} = \frac{V_{DCmax}}{\sqrt{2}}$ .

The dynamics of keeping the supercapacitor SoC constant must be much slower than the dynamics of its power control. Hence, the time constant of this control will be set around 10 sec. A PI controller will be used as an outer loop on the supercapacitor controlled variable.

For robustness, the control of the supercapacitor energy will use the DC side of the inverter when possible, and therefore the energy will be drawn from the battery. The impact of the supercapacitor energy management on the battery will be evaluated during the operation of the HESS.

As an illustration, Fig. 3.31 below shows the power of both supercapacitor and battery in two cases: with and without energy management in the supercapacitor, on a simulated event (step of angle on the network). On top of it, it shows the energy in the supercapacitor.

It can be noted that the shapes of the dynamics are almost identical as the time constant for recharging the supercapacitor (10sec) is longer than the transient dynamics of the event.

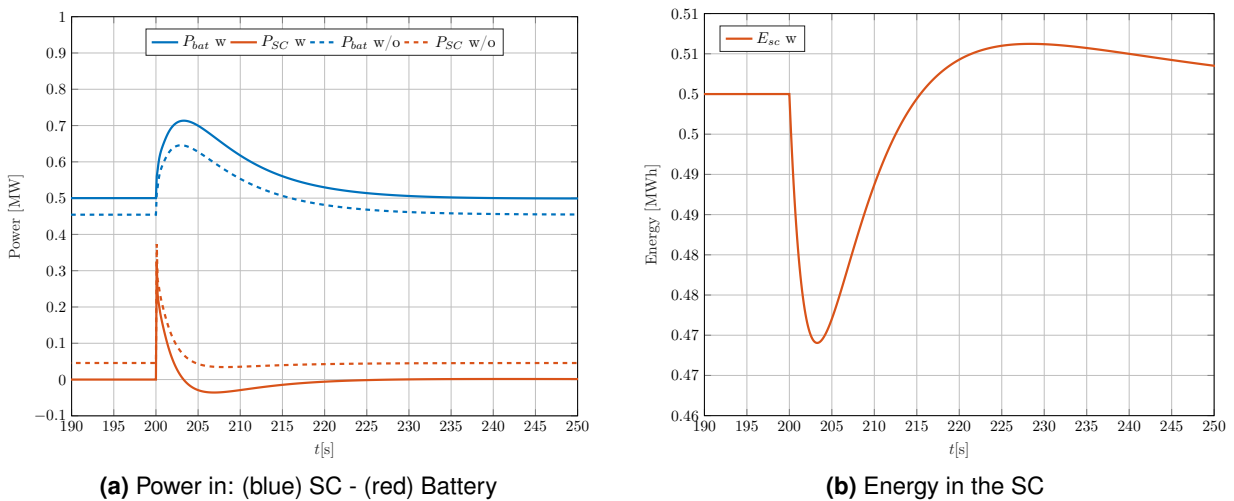


**Figure 3.31:** Angle step change with (solid line) and w/o (dotted line) Energy control

### 3.3.2.2 Energy in the Battery

In this section we will consider that the energy drawn from the battery to keep the SoC of the supercapacitor at an average value is negligible as the time constant of both storage devices are 2 orders of magnitude different. First, the SoC of the battery is not a value that can be directly measured on the device. The only physical parameter that will help describing the SoC is the voltage of the battery. Algorithms have been developed since the beginning of the use of battery to evaluate the SoC based on physical parameter and will not be discussed here. But knowing that the SoC value of the battery is just a forecast, some security margins must be taken into account in the controls. Different outer controls may be tested in the battery. For some of these controls such as virtual line and peak shaving, the future SoC is predictable and it is therefore possible to prepare a time series of Active Power setpoint that would guarantee that the battery will not go fully charged or discharged.

However, for other controls such as primary frequency control, it is not possible to know the future SoC of the battery. Therefore, it will be necessary to add a specific control that either:

- stops the battery from doing frequency control,
- have a slow outer control that brings back the energy in the battery to an average stage to ensure that it never goes to extreme SoC. Such a scheme would be similar to what was shown in Fig. 3.23 for the supercapacitor but with a much longer time scale.

### 3.3.2.3 Adaptation of frequency control for Battery energy management

Primary frequency control must be adapted to keep SoC within desirable ranges while providing this service for an undefined period of time. The proposed control is similar to one added on the supercapacitor, the idea is to regulate the average value of energy in the battery at 50% of its maximum. This can be achieved by adding an outer loop that acts on the power reference of the AC/DC inverter. The speed of this control will be set as low as possible to avoid negative effect on the overall frequency regulation. However, the proposed version does not qualify for PFC as defined in the grid code [32].

The droop of the APFC will be set at 2% for the AC/DC inverter, which means an equivalent droop of 4% as seen from the battery. For a frequency deviation of 200mHz, the battery will go to its maximum power as shown in Fig.3.32a. Having the battery at medium charge, it can handle 30 min at full charge or discharge. Therefore the dynamic of this control will be set to 30 min. It is worth noticing that a frequency deviation of 200mHz during 30 min would be a extremely unlikely event.

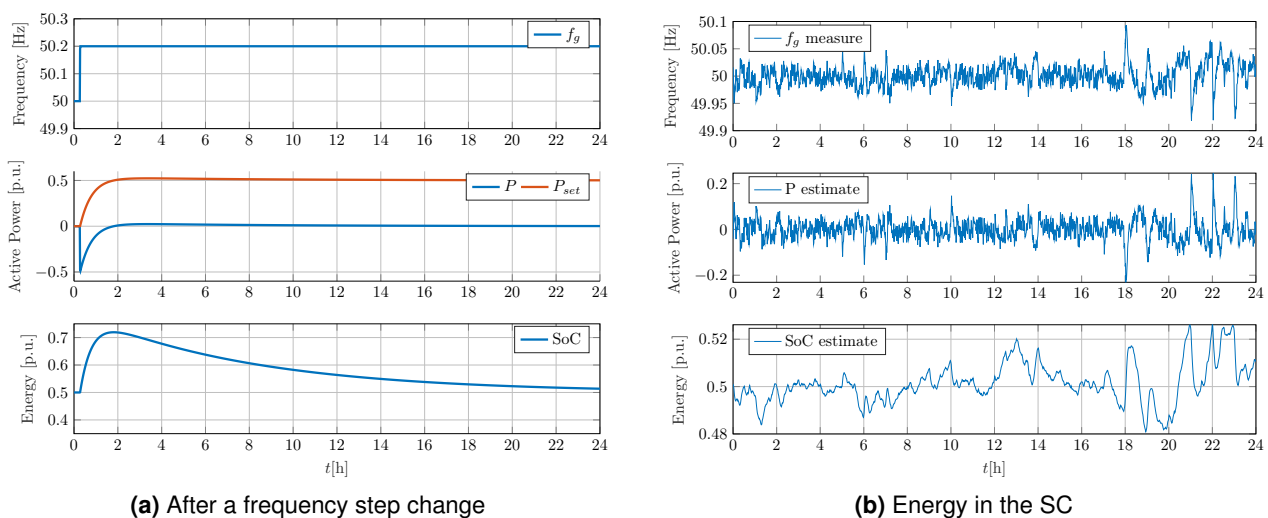


Figure 3.32: On a typical day for frequency

### 3.3.2.4 Emergency control

The value of the DC bus voltage must remain within 5% around the nominal value. If the voltage is not regulated in this band the HESS will not be able to operate and will shutdown. Such an event may be triggered by:

- a problem on the AC/DC inverter,
- a problem on the battery or on its DC/DC converter,
- a problem on the supercapacitor or on its DC/DC converter.

Different emergency action could be defined for each one of these disturbances.

For a problem on the AC/DC inverter, the HESS device will stop, the DC side must be shutdown smoothly to avoid any damage on the hardware.

For a problem on the DC/DC of the battery at least 2 solutions are possible:

- smoothly switching off the whole HESS,
- keep the HESS running, but having a very limited amount of storage (only the supercapacitor). The only service that the HESS can provide to the grid is transient grid forming (no primary/secondary frequency control can be delivered).

For a problem on the supercapacitor DC/DC, again different solutions are possible:

- smoothly switching off the whole HESS,
- keep the HESS running, but switching it to grid following control,
- keep the HESS running in grid forming mode, but pushing the fast dynamic stress on the battery.

These options and their impact on the DC side controls will be further discussed with manufacturer.

### 3.3.3 Service arbitrage for inverter capacity

For the purposes of illustration, Fig. 3.33 shows the power output of an 1 MVA inverter associated to 3 different DC systems:

- a battery (0.5MW) with a controller setting the power output at different values (both positive and negative) for defined period (blue curve).
- a supercapacitor (1MW) with a controller providing grid forming for transients (orange curve).
- a battery (0.5MW) and a supercapacitor (1MW), i.e. in RingoLab setting, with a controller that follows the power output established for the battery and provides transient grid forming.



**Figure 3.33:** Power output of an inverter providing different services.

---

It is obvious that, in the latter case, all service cannot be provided as 1.5MW of resources are connected behind a 1MW inverter. But, as the battery is not always operated at its full power, and as the grid forming induced both increase and decrease in the power, we can see in the yellow curve that most of the service is provided to the grid. In this example, the grey curve represents what would have been the power output of the inverter if it would have been of the size of the battery plus the supercapacitor (1.5MW). It is observed that the loss of grid forming service is less than 10% (the energy delivered by grid forming controls with the limitation is 90% of what it would have been without) but with investment cost significantly reduced. This behaviour will be investigated in the demonstration for the selected sizing. Here, a very basic service provided by the battery was considered for the sake of clarity, but the concept is similar with any service provided by the battery.

### 3.4 Additional grid-fault requirements

This section discusses additional requirements, besides grid forming and services listed in Table 1.1.

#### 3.4.1 Unbalance FRT requirements for grid-forming inverter

The grid-forming control developed in the MIGRATE project and to be implemented in the RingoLab HESS includes a current limiting strategy that keeps the voltage-source behavior of the converter during faults, while limiting the output current below its maximal value. The strategy was successfully validated in simulation for a three-phase fault but, as discussed in Section 3.2.3.1, appeared ineffective during single-phase fault, as the output current during this event is not bounded to the desired limit (see Fig. 3.22). However, the most probable faults in the destination grid of the storage system are single-phase. Measurement recorded on site showed that on stormy days, such as the 24th of April 2019, multiple single-phase faults can occur within one hours (the depth and the duration of a typical fault at the demo location were illustrated in Fig. 3.7). Although some grid-requirements regarding unbalance faults do exist for interfaced generation, negative sequence current injection for example [32], those FRT (fault ride through) specifications are formulated as current control problems whereas nothing as been systematically specified for voltage-controlled inverter [27].

The overall philosophy of grid-forming control for inverters is to support the grid as long as the hardware limits are not reached. Accordingly, if each phase has enough current capability, it has been suggested to maintain symmetric voltage at the converter output and feed the asymmetrical current.

If one phase-current exceeds its limit, the corresponding voltage must decrease while others should remain at nominal value, if possible. Then, the resulting control should distinguish the positive and negative sequence voltage control, or must generate each phase separately to apply the desired voltage waveforms. For consistency with previously developed control, the first approach was preferred at this stage of the design.

#### 3.4.2 Anti-islanding

Considering the grid-configuration in the substation, one have noticed that the HESS can be disconnected from the main grid and being islanded with the industrial client. One can further think that the grid-forming controlled HESS must be able to operate autonomously such islanded grid.

However, the limited capacity of the storage is not able to cope with the client needs. Also, french security rules prevent the distributed generation from staying connected after grid islanding. The same standard will then by applied to the HESS. Namely, the HESS will be disconnected if conditions provided in Table 3.4 are met (following the H4 norm in [1]).

**Table 3.4:** Anti-islanding protection for distributed generation (H4 norm, french grid-code [1] )

Trigger	Measure	Threshold	Action
$U_{min}$	Three-phase line-line voltage	80% $U_n$	Delayed 1.5 s
$U_{max}$	Single-phase line-line voltage	115% $U_n$	Delayed 0.2 s
$f_{min}$	Single-phase line-line	47 Hz	Delayed 0.5 s
$f_{max}$	Single-phase line-line	52 Hz	Delayed 0.5 s

The H4 protections are usually used for distributed generators over 5 MW because they include delayed triggers to avoid inopportune disconnection. The anti-islanding protection can be made by an external device or integrated within the HESS control. Corollary to this, the HESS control should ensure that any islanding condition will induce electrical quantities to fall above the given thresholds.

### 3.5 Test protocols

The real control codes of the fastest devices are implemented in the simulation scenario: FPGA and DSP level code. The PLC has more slow dynamics compared to the previous ones, so, a simplified version of the PLC is used in the simulation scenario. This does not affect the simulation accuracy, because the simulation run time is smaller than 20s. Once the control code has been upgraded, debugged and tested in a simulation environment, the second stage of the validation starts.

#### 3.5.1 Factory acceptance test

The same code is compiled (using another compiler) and uploaded to the CCU (Converter Control Unit) in order to verify the algorithm in a grid emulator based test bench. This time, with the real PLC code, real measurement devices, communications, real internal clock for digital devices, background code, memory mapping, etc (see Fig. 3.34).

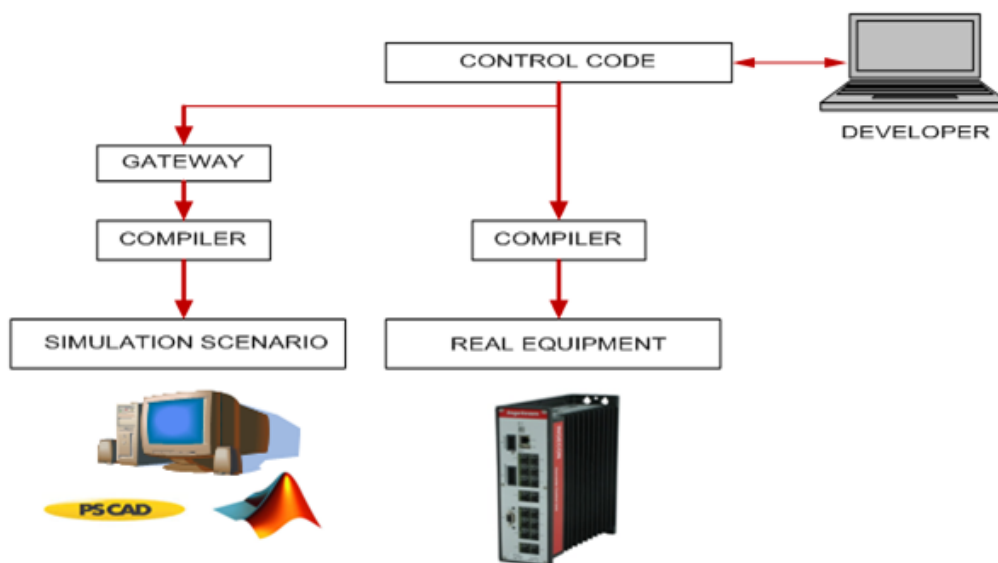


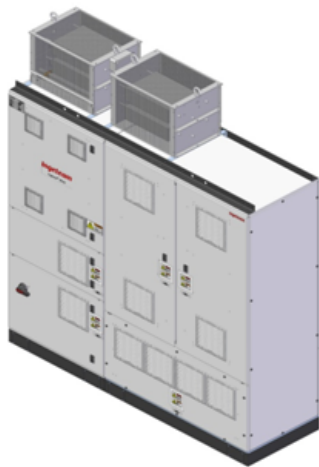
**Figure 3.34:** Main scheme of the simulation and test process

At this stage a generic validation plan (or sequence) is proposed to verify the correct integration of the new algorithm, but it can be modified depending on several factors. The planned events are:

- frequency variation,
- voltage variation,
- negative sequence,
- distorted grid (5th and/or 7th harmonic),
- voltage dips,
- phase jumps.

The biggest constraint on factory tests is space in the laboratory, since there is no room for 2 x 20' containers. Probably the lower container will be tested along with 1 supercapacitor and 1 battery rack. So, it is expected to perform these tests with a de-rating power applied to the converter. Nevertheless, depending on delivery and space issues, other ways to verify the algorithm might be used.

The power system of the grid emulator (controlled voltage source) is composed by two three level NPC converters based on IGBTs. These two converters, used as a voltage amplifier, are comprised with a front-end rectifier and a back-end inverter. Therefore, the EuT (Equipment under Test) side converter generates a predefined voltage and frequency profile, while the GSC (Grid side converter) only has the task of keeping the DC bus voltage within acceptable levels. As it is a three level NPC converter, a control technique in order to keep in balance the bus capacitors is also implemented. As the reference voltages to the EuT side converter are generated according to user specifications, the current control loops of the converter are bypassed and only the maximum current is limited with protection purposes. The characteristics of the grid emulator are shown in Fig. 3.35.



Rated Power	735 kW
Max Current	650 A
Output voltage	690 V
DC bus voltage	1100 - 1500 Vdc
Modulation	PWM 5 kHz
Cooling	water

**Figure 3.35:** Grid emulator hardware and main characteristics

### 3.5.2 On field test protocol

As the HESS is controlled as grid forming unit, most of its behavior will be guided by the network. The inverter will react to system impedance changes (load or topology), or to voltage/frequency changes. As transmission system operator, we cannot "play" with the grid topology or electrical values, and we will not be able to have specific test protocols with predefined events. Therefore, for most of the service provided by the system, we will rather measure the device behavior as well as all electrical values of the close network to be then able to characterize it. For this reason, the metrics defined in sections 2.4 and 2.5.4 will be adapted below to fit this specific situation.

### 3.6 Key performance indicators

To assess the impact of the grid forming device on the grid, a measurement campaign of both voltage and current at the connection point have started. Therefore we will be able to compare all electrical values before and after the installation of RingoLab for both normal operation and transient events.

The TFR allows recording at more than 10kHz the 3 voltages and currents for 10 sec. The recording is triggered for different events like phase shift or voltage amplitude step. The metrics defined for the demonstration in EPFL environment will be slightly modified and also other metrics will be used. Below will be presented the different metrics for the different service that will be tested on RingoLab:

- **Frequency smoothing.** The effect of the device on the frequency will be evaluated on the real system by correlating the frequency deviation events to the load variations given by the active power changes of the customer. For this purpose,  $metric_2$  and  $metric_3$  will be redefined on the basis of a statistical analysis of their sensitivity to all active power step change  $\Delta P$ . Hence:

The indicator  $metric_{2a} = \frac{RoCoF}{\Delta P}$  will be used before and after installation.

The indicator  $metric_{3a} = \frac{Nadir}{\Delta P}$  will be used before and after installation.

- **Voltage amplitude smoothing:** Analogously,  $metric_4$  will be redefined considering the correlation between the voltage amplitude variation to a load change event. Then, for all active power step change  $\Delta P$ , the voltage amplitude change  $\Delta V$  will be calculated as follow:  
 $metric_{4a} = \frac{\Delta V}{\Delta P}$ .

Indeed, the behavior of the grid forming being a voltage source in steady state, the voltage is expected to be stiffer after the installation of the grid forming inverter.

- **Battery output smoothing.** In order to quantify the smoothing effect brought by the use of the supercapacitance, the derivative of the power of both the battery and the supercaps will be measure and compared for each event:

$$metric_7 = \frac{P_{SC}}{P_{Batt}} \frac{\frac{\Delta P_{Batt}}{dt}}{\frac{\Delta P_{SC}}{dt}}$$

- **Effective current limitation during transients.** During the testing period of the grid forming inverter, it will be checked that in any condition, the output current of the inverter does not overpass the defined limitation threshold. The proposed indicator is the number of occurrence of hardware IGBT blocking due to overcurrent:  $metric_8 = n_{occurrence}$ .
- **DC storage.** The effectiveness of the DC side energy management strategies in preventing the supercapacitor to go empty or fully charged ( $0 < SOC_{SC} < 1$ ) will be quantified. Having such a situation would lead to a global system that would behave as grid following or to a system that would put all the stress of grid forming behavior on the battery
- **Service limitation.** As stated in the description of the HESS, the sum of the power available on the DC side is bigger that the power capability of the DC/AC inverter. Therefore there might be some cases where the AC/DC inverter will limit the current, the duration of this limitation will be an indicator of how well suited are the combination of the different services. The limitation will occur when power from grid forming control and battery control will be above the nominal power of the inverter. The power from grid forming control only depends on the system variations and cannot be changed. The power output from battery control will depend on the provided service (primary/secondary control or peak shaving). The metric will be the amount of energy non delivered to the grid due to the AC/DC power limitation:  $metric_9 = \frac{Energy_{nondelivered}}{TotalEnergy_{delivered}}$

Fair comparison of the frequency event prior and after the installation of the grid forming device will be ensured by using the same PMU for the frequency calculation, which was developed by EPFL [8].

## 4 Conclusion

The deliverable D3.2 of OSMOSE WP3 gathers, in a synthetic form, all the information to make the demonstrators as transparent and reproducible as possible. In the two demonstrations in parallel, one in EPFL (Lausanne, Switzerland), one in the south of France (Luzenac, France), the main goal is to test grid-forming effectiveness on grid quantities, robustness against grid events, portability over different hardware platform, cost efficiency through multi-services optimization. Though, the focus is put on different aspects.

In EPFL, converting the 640kW BESS demonstrator to include the grid-forming functionality is very challenging, as the system is already built with limited access to internal control and to the manufacturer intellectual property. However the EPFL can rely on two advantages. The surrounding grid is meshed with proprietary PMUs measurements of high accuracy, and the BESS itself is backed with powerful study tools. In configurable microgrid with a reduced size replica of the BESS that is fully controllable, the researchers are able to compare the real size achievements with ideal results. Besides, a real-time simulation of a 39-bus network can expand the results to a scaled-up solution where multi-service storage system can now be taken into account.

In the south of France, the demonstrator will be operated under transmission grid conditions with varying client, production and (relatively) weak grid at the point of common coupling. The challenge of Ringolab will be the grid-forming control improvements from Ingeteam to meet grid conditions with existing hardware constraints. Particularly, the unbalanced robustness is of major importance. Regarding the DC energy management strategy, propositions have been made to temporally separate the grid services but also physically distinguish the DC hardware affected to a dedicated service. To our opinion, these developments are inevitable steps toward the future application of grid-forming in the system.

In the document the emphasis has been put on critical challenges in the future demonstrators design, and on the expected experimental and supporting simulation results. During the upcoming year, the interested reader should pay attention to the next project outputs:

- The opportunity to convert an existing grid-following BESS into grid-forming, with the related technical and economical cost, and the expected effectiveness.
- The potential of scaling up the BESS solution with grid-forming and multi-service on a large system to maintain frequency quality and to resist islanding.
- The chosen DC management strategy that will seamlessly switch from one ancillary service to another, from one DC storage device, to another.
- The factory acceptance tests of Ingeteam that will definitely validate the grid-forming control compatibility with existing hardware.
- The first line fault where the HESS of Ringolab is asked to stay connected and feed the fault as much as possible.
- The measurement technique based on EPFL PMU technology to assess the frequency smoothing capability, also called synchronization service.

## Bibliography

- [1] ENEDIS. [Online]. Available: [https://www.enedis.fr/sites/default/files/Enedis-NOI-RES\\_13E.pdf](https://www.enedis.fr/sites/default/files/Enedis-NOI-RES_13E.pdf)
- [2] M. L2EP, 2018. [Online]. Available: [https://www.h2020-migrate.eu/\\_Resources/Persistent/5c5beff0d5bef78799253aae9b19f50a9cb6eb9f/D3.2-%20-%20Local%20control%20and%20simulation%20tools%20for%20large%20transmission%20systems.pdf](https://www.h2020-migrate.eu/_Resources/Persistent/5c5beff0d5bef78799253aae9b19f50a9cb6eb9f/D3.2-%20-%20Local%20control%20and%20simulation%20tools%20for%20large%20transmission%20systems.pdf)
- [3] M. ETHZ, 2018. [Online]. Available: [https://www.h2020-migrate.eu/\\_Resources/Persistent/0298d5d56a3f1977e8b95e5476a88a7b840004cf/D3.3-%20-%20New%20options%20for%20existing%20system%20services%20and%20needs%20for%20new%20system%20services.pdf](https://www.h2020-migrate.eu/_Resources/Persistent/0298d5d56a3f1977e8b95e5476a88a7b840004cf/D3.3-%20-%20New%20options%20for%20existing%20system%20services%20and%20needs%20for%20new%20system%20services.pdf)
- [4] E. Namor, “Advanced models and algorithms to provide multiple grid services with battery storage systems,” 2018. [Online]. Available: <http://infoscience.epfl.ch/record/256959>
- [5] M. Pignati, M. Popovic, S. Barreto, R. Cherkaoui, G. Dario Flores, J. Le Boudec, M. Mohiuddin, M. Paolone, P. Romano, S. Sarri, T. Tesfay, D. Tomozei, and L. Zanni, “Real-time state estimation of the epfl-campus medium-voltage grid by using pmus,” in *2015 IEEE Power Energy Society Innovative Smart Grid Technologies Conference (ISGT)*, Feb 2015, pp. 1–5.
- [6] K. Strunz, “Cigrè task force c6.04.02 - benchmark systems for network integration of renewable and distributed energy resources,” July 2009.
- [7] P. Romano and M. Paolone, “Enhanced interpolated-dft for synchrophasor estimation in fpgas: Theory, implementation, and validation of a pmu prototype,” *IEEE Transactions on Instrumentation and Measurement*, vol. 63, no. 12, pp. 2824–2836, Dec 2014.
- [8] P. Romano, M. Pignati, and M. Paolone, “Integration of an IEEE Std. C37.118 compliant PMU into a real-time simulator,” in *2015 IEEE Eindhoven PowerTech*, June 2015, pp. 1–6.
- [9] T. Marthworks, “Simpowersystems 4 – reference manual, the mathworks, inc., natick, massachusetts, 2007.”
- [10] “Dynamic models for steam and hydro turbines in power system studies,” *IEEE Transactions on Power Apparatus and Systems*, no. 6, pp. 1904–1915, 1973.
- [11] “IEEE draft recommended practice for excitation system models for power system stability studies,” *IEEE P421.5/D38*, October 2015, pp. 1–202, Jan 2015.
- [12] I. working group, “Hydraulic turbine and turbine control models for system dynamic studies,” *IEEE Transactions on Power Systems*, vol. 7, no. 1, pp. 167–179, Feb 1992.
- [13] “Load representation for dynamic performance analysis (of power systems),” *IEEE Trans on Pow Sys*, vol. 8, no. 2, pp. 472–482, May 1993.
- [14] A. Derviškić, P. Romano, M. Pignati, and M. Paolone, “Architecture and experimental validation of a low-latency phasor data concentrator,” *IEEE Trans on Smart Grid*, vol. 9, no. 4, pp. 2885–2893, July 2018.
- [15] R. Version, “8.1 user guide,” *Opal-RT Technologies INC*, 2007.
- [16] H. W. Dommel, “Digital computer solution of electromagnetic transients in single-and multiphase networks,” *IEEE Transactions on Power Apparatus and Systems*, vol. PAS-88, no. 4, pp. 388–399, April 1969.
- [17] C. Dufour and J. Belanger, “A real-time simulator for doubly fed induction generator based wind turbine applications,” in *2004 IEEE 35th Annual Power Electronics Specialists Conference (IEEE Cat. No.04CH37551)*, vol. 5, June 2004, pp. 3597–3603 Vol.5.
- [18] R. Pena, J. C. Clare, and G. M. Asher, “Doubly fed induction generator using back-to-back pwm converters and its application to variable-speed wind-energy generation,” *IEE Proceedings - Electric Power Applications*, vol. 143, no. 3, pp. 231–241, May 1996.

- 
- [19] GE Energy, "Analysis of wind generation impact on ercot ancillary services requirements," 2008.
- [20] K. Coughlin and J. H. Eto, "Analysis of wind power and load data at multiple time scales," Lawrence Berkeley National Laboratory (LBNL), Berkeley, CA (United States), Tech. Rep., 2010.
- [21] G. Denis, T. Prevost, M. Debry, F. Xavier, X. Guillaud, and A. Menze, "The migrate project: the challenges of operating a transmission grid with only inverter-based generation. a grid-forming control improvement with transient current-limiting control," *IET Renewable Power Generation*, vol. 12, no. 5, pp. 523–529, 2018.
- [22] F. Sossan, E. Namor, R. Cherkaoui, and M. Paolone, "Achieving the dispatchability of distribution feeders through prosumers data driven forecasting and model predictive control of electrochemical storage," *IEEE Transactions on Sustainable Energy*, vol. 7, no. 4, pp. 1762–1777, Oct 2016.
- [23] C. Dufour, J. Mahseredjian, and J. Belanger, "A combined state-space nodal method for the simulation of power system transients," *IEEE Transactions on Power Delivery*, vol. 26, no. 2, pp. 928–935, April 2011.
- [24] RTE, 2013. [Online]. Available: [http://clients.rte-france.com/htm/fr/mediatheque/telecharge/reftech/03-05-13\\_complet.pdf](http://clients.rte-france.com/htm/fr/mediatheque/telecharge/reftech/03-05-13_complet.pdf)
- [25] PQIDA, 2019. [Online]. Available: <https://www.a-eberle.de/en/product-groups/pq-fix-installed/devices/pqi-da-smart>
- [26] T. Qoria, T. Jouini, D. Gross, U. Markovic, G. Denis, and T. Prevost, "Data underlying the research of a 3 bus model for full inverter system - migrate wp3," 2018. [Online]. Available: <https://doi.org/10.4121/uuid:e5497fd2-f617-4573-b6d5-1202ebae411d>
- [27] P. Piya, M. Ebrahimi, M. Karimi-Ghartemani, and S. A. Khajehoddin, "Fault Ride-Through Capability of Voltage-Controlled Inverters," *IEEE Transactions on Industrial Electronics*, vol. 65, no. 10, pp. 7933–7943, 2018.
- [28] T. Zheng, L. Chen, Y. Guo, and S. Mei, "Comprehensive control strategy of virtual synchronous generator under unbalanced voltage conditions," *IET Generation, Transmission & Distribution*, vol. 12, no. 7, pp. 1621–1630, 2017.
- [29] X. Guo, W. Liu, X. Zhang, X. Sun, Z. Lu, and J. M. Guerrero, "Flexible control strategy for grid-connected inverter under unbalanced grid faults without PLL," *IEEE Transactions on Power Electronics*, vol. 30, no. 4, pp. 1773–1778, 2015.
- [30] L. Kouchachvili, W. Yaïci, and E. Entchev, "Hybrid battery/supercapacitor energy storage system for the electric vehicles," *Journal of Power*, vol. 374, p. 237–248, 01 2018.
- [31] C. Capasso and O. Veneri, "Integration between super-capacitors and zebra batteries as high performance hybrid storage system for electric vehicles," *Energy Procedia*, vol. 105, pp. 2539 – 2544, 2017, 8th International Conference on Applied Energy, ICAE2016, 8-11 October 2016, Beijing, China. [Online]. Available: <http://www.sciencedirect.com/science/article/pii/S1876610217307907>
- [32] ENTSOE, "Rfg grid code," 2016. [Online]. Available: [https://eur-lex.europa.eu/legal-content/EN/TXT/?uri=OJ:JOL\\_2016\\_112\\_R\\_0001#d1e2484-1-1](https://eur-lex.europa.eu/legal-content/EN/TXT/?uri=OJ:JOL_2016_112_R_0001#d1e2484-1-1)

